^{77}Se NMR Spectroscopic, DFT MO, and VBT Investigations of the Reversible Dissociation of Solid $(Se_6I_2)[AsF_6]_2 \cdot 2SO_2$ in Liquid SO_2 to Solutions Containing 1,4–$Se_6I_2^{2+}$ in Equilibrium with Se_n^{2+} (n = 4, 8, 10) and 7 Binary Selenium Iodin cations. Preliminary Evidence for 1,1,4,4–$Se_4Br_4^{2+}$ and *cyclo*–Se_7Br^+.

Scott Brownridge,[†] Larry Calhoun,[†] H. Donald B. Jenkins,*[,¶] Risto S. Laitinen,*[,‡] Michael P. Murchie,[†] Jack Passmore,*[,†] Jarkko Pietikäinen,[‡] J. Mikko Rautiainen,[&] Jeremy C.P. Sanders,[†] Gary J. Schrobilgen,[§] Reijo J. Suontamo,[&] Heikki M. Tuononen,[&] Jussi U. Valkonen,[&] and Chi-Ming Wong [†]

Departments of Chemistry, University of New Brunswick, #45222, Fredericton, NB, E3B 6E2, Canada, University of Warwick, Coventry CV4 7AL, West Midlands, United. Kingdom,. University of Oulu, P.O. Box 3000, FI-90014 Oulu, Finland, University of Jyväskylä, P.O. Box 35, FI-40014 Jyväskylä, Finland, and McMaster University, Hamilton, Ontario, L8S 3M1, Canada.

	Solid state thermodynamics	NMR spectroscopy DFT modelling	Problem conception Solution development Overall chemistry
E-mail:	h.d.b.jenkins@warwick.ac.uk	risto.laitinen@oulu.fi	passmore@unb.ca
Tel:	(44)2476-523265 or (44)2476-466747	(3588)553-1611	(506)453-4821
Fax:	(44) 2476 524112	(3588) 553-1603	(506) 453-4981

[†] University of New Brunswick, [¶] University of Warwick, [‡] University of Oulu, [&] University of Jyväskylä, [§] McMaster University

Abstract

The composition of a complex equilibrium mixture formed upon dissolution of $(Se_6I_2)[AsF_6]_2 \bullet 2SO_2$ in SO_2(l) was studied by ^{77}Se NMR spectroscopy at –70 ^{o}C with both natural-abundance and enriched ^{77}Se-isotope samples (enrichment 92 %). Both the natural-abundance and enriched NMR spectra showed the presence of previously known cations 1,4-$Se_6I_2^{2+}$, SeI_3^+, 1,1,4,4-$Se_4I_4^{2+}$, Se_{10}^{2+}, Se_8^{2+}, and Se_4^{2+}. The structure and bonding in 1,4-$Se_6I_2^{2+}$ and 1,1,4,4-$Se_4I_4^{2+}$ were explored by DFT calculations. It was shown that the observed Se-Se bond alternation and presence of thermodynamically stable 4pπ-4pπ Se-Se and 4pπ-5pπ Se-I bonds arise from positive charge delocalization from the formally positively charged tricoordinate Se^+. The ^{77}Se chemical shifts for cations were calculated using the relativistic zeroth-order regular approximation (ZORA). In addition, calculations adding a small number of explicit solvent molecules and an implicit Conductor-like Screening Model (COSMO) were conducted to include the effect that solvent has on the chemical shifts. The calculations yielded a reasonable agreement with experimental chemical shifts and inclusion of solvent effects was shown to improve the agreement over vacuum values. The ^{77}Se NMR spectrum of the equilibrium solution showed 22 additional resonances. These were assigned based on ^{77}Se-^{77}Se COSY, selective irradiation experiments, and spectral simulation. By combining this information with the trends in the chemical shifts, with iodine, selenium, and charge balances, as well as with ZORA chemical shift predictions, these resonances were assigned to acyclic 1,1,2-$Se_2I_3^+$, 1,1,6,6-$Se_6I_4^{2+}$, and 1,1,6-$Se_6I_3^+$, as well as to cyclic Se_7I^+ and (4-$Se_7I)_2I^{3+}$. A preliminary natural-abundance ^{77}Se NMR study of the soluble products of the reaction of $(Se_4)[AsF_6]_2$ and bromine in liquid SO_2 included resonances attributable to 1,1,4,4-$Se_4Br_4^{2+}$. These aassignments are supported by the agreement of the observed and calculated ^{77}Se chemical shifts. Resonances attributable to cyclic Se_7Br^+ were also observed. The thermal stability of $(Se_6I_2)[AsF_6]_2 \bullet 2SO_2$(s) was consistent with estimates of

thermodynamic values obtained by Volume Based Thermodynamics (VBT) and the first application of the Thermodynamic Solvate Difference Rule for non-aqueous solvates. $(Se_6I_2)[AsF_6]_2 \bullet 2SO_2(s)$ is the first example of an SO_2 solvate for which the non-solvated parent salt, $(Se_6I_2)[AsF_6]_2(s)$ is *not* thermodynamically stable disproportionating to $Se_4I_4(AsF_6)_2(s)$ and $Se_8(AsF_6)_2(s)$ (ΔG^o for the disproportion reaction is estimated to be – 17 ± 15 kJ mol^{-1} at 298 K from VBT theory).

Introduction

Sulfur-iodine and selenium-iodine covalent 2c-2e bonds in neutral compounds are thermodynamically unstable under ambient conditions.[1] The instability of the S–I and Se–I bonds has been attributed to their very low ionic resonance stabilization energies because of the similar electronegativities of iodine and sulfur or selenium. In the solid state, the interconversion of two E–I (E = S or Se) bonds into E–E and I–I bonds is further facilitated by the large sublimation energy of solid iodine (62.3 kJ mol^{-1}).[2]

The successful preparation and characterization of $(C_5H_5NH)_2[SeI_6]$ [3a] in the 1960's and that of $(SeI_3)[AsF_6]$ in 1970's [3b] initiated rapid progress in the chemistry of species containing Se–I covalent bonds (see Table 1). The stability of these binary selenium–iodine containing ions is attributed, in part, to the lattice energy of the corresponding salt.[1a,19] The number, range and novelty of the bonding in these selenium–iodine species is now comparable to that of the binary sulfur and selenium fluorides.[1,44]

Most of the chalcogen–halogen cations have been identified in the solid state and characterized by single crystal X–ray crystallography. However the speciation is not necessarily the same in solution, especially in the case of dications which are generally thermodynamically unstable in the gas phase.[44,45] For example, solid $(S_3N_2)[AsF_6]_2$ completely dissociates in liquid SO_2 to give SN^+, SNS^+, and $2AsF_6^-$ ions,[46] and solid $(S_8)[AsF_6]_2$ forms 2 $[AsF_6]^-$ and S_8^{2+} in equilibrium with S_5^+ and ½ S_6^{2+}, a consequence of the difference in the energetics in the solid state and in solution.[47] In this paper the behavior of $(Se_6I_2)[AsF_6]_2{\cdot}2SO_2$ in solution is explored by selenium NMR spectroscopy. $(Se_6I_2)[AsF_6]_2{\cdot}2SO_2$ was first prepared in 1985 and its solid state structure was shown to contain 2 $[AsF_6]^-$ anions and $Se_6I_2^{2+}$ cations with weak cation–anion contacts.[22] The structure of $Se_6I_2^{2+}$ is given in Figure 1 and includes pertinent bond distances. The cation contains

tricoordinate selenium atoms that are formally positively charged, strong selenium–selenium bond alternation, thermodynamically stable 4pπ–4pπ Se–Se and 4pπ–5pπ Se–I bonds, and has an over all distorted cubic cluster–like geometry, all common features of this cation class. It has been proposed that these structural features arise from positive charge delocalization from the formally positively charged tricoordinate chalcogen onto all atoms in the molecule, thus minimizing positive charge repulsion. For $Se_6I_2^{2+}$ these bonding and structural features were accounted for qualitatively by valence bond structures as shown in Figure 2.[22]

Natural abundance ^{77}Se NMR studies showed that solid $(Se_6I_2)[AsF_6]_2 \cdot 2SO_2$ dissolved in liquid SO_2 to give solvated $Se_6I_2^{2+}$ in equilibrium with solvated Se_8^{2+} and solvated $Se_4I_4^{2+}$, as shown in equation (1), and smaller amounts of some other selenium containing species.[22]

$$2\ Se_6I_2^{2+}(solv) \leftrightharpoons Se_4I_4^{2+}(solv) + Se_8^{2+}(solv) \qquad (1)$$

NMR studies also showed that solvated ions $Se_6I_2^{2+}$ and SeI_3^+ were the products of the dissociation of $Se_4I_4^{2+}$ in liquid SO_2 according to equation (2), given on reaction of $(Se_4)[AsF_6]_2$ and I_2 in SO_2 solution.[21]

$$2\ Se_4I_4^{2+}(solv) \leftrightharpoons Se_6I_2^{2+}(solv) + 2\ SeI_3^+(solv) \qquad (2)$$

The natural–abundance ^{77}Se NMR data for $Se_6I_2^{2+}$ [21] was consistent with the structure observed in the solid state,[22] though the resonances could be assigned in terms of both *exo,exo*–1,4,–$Se_6I_2^{2+}$ and *endo,endo*–1,4–$Se_6I_2^{2+}$ structures. In case of $Se_4I_4^{2+}$ the natural–abundance ^{77}Se NMR information indicated an AMM'A' chain $I_2SeSeSeSeI_2^{2+}$ structure.[22]

In an attempt to determine the nature of several other species, the ^{77}Se NMR spectrum of a $Se_6I_2^{2+}$ sample enriched to 92 % ^{77}Se was prepared. In this paper we describe a detailed

analysis of the resulting complex but rich spectrum in a quest to identify the unknown dissociation products of $Se_6I_2^{2+}$ in SO_2 solution. Preliminary results have been published.[48]

In order to assign the complex ^{77}Se NMR spectra we obtained the first 2D ^{77}Se–^{77}Se COSY spectrum to be reported, to the best of our knowledge. We also carried out complementary homonuclear solution ^{77}Se–^{77}Se decoupling experiments and careful resonance intensity measurements.

^{77}Se chemical shifts of several selenium compounds have been calculated with good accuracy by using non–relativistic DFT methods.[49] Demko *et al.*[50] have calculated relativistic ^{77}Se chemical shifts on several organic, organometallic, and inorganic selenium containing compounds using ZORA DFT calculations and compared them to solid state ^{77}Se NMR results. They concluded that inclusion of relativistic contributions to calculated ^{77}Se chemical shifts becomes warranted if selenium is bound to an element heavier than itself. Apart from our preliminary theoretical account [51] no chemical shift calculations involving species with selenium bound to iodine have been reported so far, but Tattershall and Sandham [52] have used low level (RHF/3–21G*) results to confirm the assignment of observed ^{77}Se chemical shifts to exo,exo–α–(P_4Se_3)[CN]I by empirically fitting the calculated ^{77}Se chemical shifts of similar P_4Se_3XY compounds to experimental chemical shifts. Therefore, encouraged by these successes in calculating ^{77}Se chemical shifts, we carried out DFT studies in order to confirm the solution structures of the known $Se_6I_2^{2+}$ and $Se_4I_4^{2+}$ and to aid the identification of the unknown selenium species. We note that no salts containing $Se_4I_4^{2+}$ have been isolated. Crystals obtained from solutions of $(Se_4I_4)[AsF_6]_2$ prepared *in situ*, were either $(SeI_3)[AsF_6]$ or $(Se_6I_2)[AsF_6]_2.2SO_2$ i.e. the $[AsF_6]^-$ salts of the products of dissociation of $Se_4I_4^{2+}$ in solution as given in Equation 2.[21,53] DFT calculations were used to determine the nature of the bonding in $Se_6I_2^{2+}$ and $Se_4I_4^{2+}$, to account for their structures, and to test the validity of previously proposed simple qualitative bonding models.[1,22] This is the first quantitative study

of the bonding of a typical halo–polychalcogen cation. The only related work is the theoretical investigation of the, rather different, $M_2I_4^{2+}$(M = S, Se) [54] and the homopolyatomic cations M_n^{2+} (n=4, M = S, Se, Te ;[55] n = 8, M = S, Se [45])

VBT calculations [56,57] and the Thermodynamic Solvate Difference Rule [58].have been combined to assist with the estimation of the thermochemistry. This is the first time the two approaches have been used together. As an evolving method the use of this approach shows considerable promise for use in exploring the thermochemistry of non–aqueous systems.

We also report a natural–abundance ^{77}Se NMR study of the reaction of Se_4^{2+} and Br_2 leading to several new selenium species. We identified 1,1,4,4–$Se_4Br_4^{2+}$ by comparison of its chemical shifts with that of $Se_4I_4^{2+}$ and related selenium iodine cations, and the DFT calculated ^{77}Se chemical shifts, and tentatively assigned cyclo–Se_7Br^+ in the reaction products, both of which were hitherto unknown. This preliminary result, and the NMR investigations of $Se_6I_2^{2+}$ in solution implies that there is a large number of halidoselenium binary halide cations to be included in the family of the chalcogen halides (see Table 1 and Supporting Information).

Experimental Section

The preparation of samples of $(Se_6I_2)[AsF_6]_2{\cdot}2SO_2$ in SO_2 solution for NMR studies. Apparatus, techniques, and chemicals used in this work have been described elsewhere,[3,59] except where stated. $(Se_6I_2)[AsF_6]_2{\cdot}2SO_2$ was prepared from elemental selenium, iodine, and arsenic pentafluoride in rigorously anhydrous conditions, as described previously.[22] Two samples were prepared, one involving natural–abundance selenium and the other selenium enriched in the ^{77}Se–isotope (Techsnabexport, enrichment 92 %). The ^{77}Se–enriched sample was prepared *in situ* in a thick walled 10 mm NMR tube by condensing 0.1101 g (0.648

mmol) of AsF_5 onto a mixture of 0.0970 g (1.260 mmol) of ^{77}Se–enriched selenium and 0.0535 g (0.211 mmol) of iodine in 2.33 cm^{-3} of liquid SO_2 resulting in a solution with 0.5 mol dm^{-3} of ^{77}Se. After the synthesis, the NMR tube was flame sealed and agitated in a sonic bath at 30–35 ^oC [60] before recording the ^{77}Se NMR spectrum. Solid $(Se_6I_2)[AsF_6]_2 \cdot 2SO_2$ precipitates from solution after cooling to –80 C on standing at RT for some time.[22b,c] Therefore samples were always resonicated prior to obtaining each NMR spectrum. The preparation of the natural–abundance sample was carried out following the procedure reported previously.[22b]

Reaction of $(Se_4)[AsF_6]_2$ and Br_2 in Liquid SO_2. ($Se_4)[AsF_6]_2$ prepared as described previously [61] was reacted with bromine (Fischer Scientific, stored over P_2O_5) in 10mm NMR tubes equipped with a Teflon in glass valve (J. Young, O–ringette PTFE stopcock). An intense red–brown solution was formed over solids in all cases. The reactant weights and identity of the insoluble solids are given in Table 2. Full details are given in Ref. 53.

NMR Spectroscopy. The $(Se_6I_2)[AsF_6] \cdot 2SO_2$ ^{77}Se NMR spectra were recorded in SO_2(l) at –70 ^oC employing Bruker DSX300 and Varian UNITY 400 spectrometers operating at 57.24, and 76.27 MHz, respectively, using the spectral widths of 100,000 Hz unless specified otherwise.[63] The respective pulse widths were 6.0 and 15.8 μs corresponding to nuclear tip angles of 42 and 45°, respectively. Acetone–d_6 was used as an external ^{2}H lock and the spectra were referenced to neat $(CH_3)_2Se$ at 298 K. No temperature correction was applied. Variable temperature units were calibrated using a standard methanol sample.

The natural–abundance ^{77}Se NMR spectra of the samples from the reaction of $(Se_4)[AsF_6]_2$ and Br_2 in liquid SO_2 were obtained using a Varian XC200 spectrometer and a 10mm broad band probe (frequency range 20 to 80 MHz) tuned to 63.194 MHz. Spectral width settings of 50 and 100 kHz were employed with digital resolution of 6.1 Hz and

acquisition times of 0.164 s and a pulse width of 23.0 μs. Solids were isolated by pouring off the supernatant solution by use of an NMR tube adapter.[59c]

Correlations between the ^{77}Se resonances *via* *J*–couplings were determined using homonuclear ^{77}Se–^{77}Se magnitude mode COSY and Phase–Sensitive Double–Quantum–Filtered COSY (PS–DQF COSY) experiments on a Bruker DSX300 spectrometer. Typically, 576 transients were collected for each of 300 time increments (150 complex points) with two– or four–fold linear prediction. The pulse width was 13.0 μs, corresponding to the nuclear tip angle of 90°. Spectral widths in F1 and F2 were 100,000 Hz with an acquisition time of 0.005 s and a relaxation delay of 0.150 s. Correlations were confirmed and extended to smaller *J*–couplings by performing a series of homonuclear ^{77}Se–^{77}Se decoupling experiments using the dual–broad band Varian UNITY 400 spectrometer. Relaxation times were measured by fitting signal amplitudes of spectra recorded using the inversion–recovery pulse sequence with single exponentials using standard Varian VNMR software (Version 4.3 Revision A). Typical t_1 relaxation times were 0.110(5) s on a 400 MHz instrument. The t_1 relaxation times seemed to be similar for all resonances and were independent on the field strength.

Relative ^{77}Se signal intensities were quantified using a series of spectra recorded with a Varian UNITY 400 spectrometer. Relaxation delay of 0.35 s and acquisition time of 0.25 s were used in the measurements. Variations in signal intensities arising from non–uniform pulse power distributions was minimized by using a pulse width of 15.8 μs, corresponding to the nuclear tip angle of 45° and adjusting the transmitter offset to place each integrated signal in turn within the central 10,000 Hz of the spectral width.[64]

Spectral simulations were carried out by using the programs PERCH [65] and ISOTOPOMER.[66] The coupling constants for different molecular species were determined and refined using program PERCH by fitting the observed transition patterns to those profiles calculated for the isotopomer of each cation that contains the ^{77}Se–nucleii in all selenium

positions. The program ISOTOPOMER was then utilized in calculating the effects of the presence of other isotopomers in the resonances utilizing the refined coupling constants.

Computational Details

All geometry optimizations were performed with Turbomole 5.9 program package [67] at hybrid DFT level of theory employing PBE0 functional.[68] Dunning's correlation consistent cc–pVTZ [69] and effective large core potential SDB–cc–pVTZ [70] basis sets were utilized in optimizations for selenium and iodine atoms respectively. This combination of basis sets is denoted as (SDB)–cc–pVTZ. The natures of the optimized stationary points were confirmed with subsequent frequency calculations. Relative gas phase energies of the structures were determined with CCSD(T)/(SDB)–cc–pVTZ single point calculations on DFT optimized geometries using Molpro 2002.6 program.[71] To test the validity of the DFT structures some of the cations were also optimized with MP2 method. The MP2 optimized structures did not significantly differ from the DFT optimized, though the Se…Se and Se…I contacts were shorter with MP2 than by using DFT. The MP2 optimized contacts were better in agreement with those observed in the solid state. However, the calculated CCSD(T) energies for MP2 structures were higher than those calculated for DFT optimized structures; the chemical shifts calculated for MP2 optimized structures were also further away from experimental chemical shifts. This suggests that the long contacts have minor significance to the calculated shielding constants and supports using DFT structures for chemical shift calculations (for further details of MP2 calculations, see the Supporting Information). The conductor–like screening (COSMO) model [72] implemented in Turbomole program was employed to obtain solvation energies. Solvent radius (R_{solv} = 2.032 Å) and dielectric constant [ε(–70 °C) = 24] [73] were used as parameters for COSMO. Natural orbital analyses were obtained using the NBO

program (version 5.0) [74] and properties of the atoms in molecules bond critical points were calculated with AIMPAC.[75]

The ^{77}Se chemical shift calculations were carried out at a relativistic level by using the two–component zeroth–order regular approximation (ZORA) method with spin–orbit corrections [76] implemented in the ADF program package.[77] The ZORA NMR calculations employed the rPBE GGA functional [68a,78] and large QZ4P basis sets, as implemented in the ADF internal basis set library. The staggered–staggered conformation of $SeMe_2$ was adopted as the chemical shift reference point in a similar manner to previous studies.[79] The calculated isotropic shielding tensor used for the reference was 1794.6 ppm.

For the explicit solvent calculations the structures of the cation–solvent clusters were optimized using a resolution of identity approximation [80] with the PBE0 functional and def2–TZVP basis set for all elements, as implemented in Turbomole program package.[80,81] The chemical shift calculation was then carried out analogously to the vacuum calculation, but a smaller TZP basis set was used for the solvent SO_2 molecules and the COSMO model was used to include the continuum solvent effects. The reference $SeMe_2$ for the explicit solvent calculations was calculated with the COSMO model but without explicit SO_2 molecules. The isotropic shielding tensor that was used for the $SeMe_2$ reference in explicit solvent calculations was 1829.1 ppm.

Computational Thermochemistry. Supporting Information to this paper explains the detailed calculations that appear elsewhere and should be read in conjunction with the main text. There are no experimental thermochemical data available of any kind for the selenium compounds considered in this paper. However we have access to gas–phase thermodynamic calculations (results appear in Table 6 and Table S4 in Supporting Information.) and thermodynamic data for the solid state can be obtained using our VBT, the volume–based approach [56-58] (see also Supporting Information).

In addition to solid state reactions of normal salts, this paper also requires us to consider thermodynamics of solvates, viz. $(Se_6I_2)[AsF_6]_2.2SO_2$ and $Se_8[AsF_6]_2$ $\frac{1}{3}SO_2$. Prior to present work there has been no requirement to extend the VBT approach to make predictions of the energetics (thermodynamics) of salts containing non–aqueous solvent molecules. Thus the study of the solvated selenium salts in this paper represents the very first of its kind.

In this context we need to consider reactions such as:

$$(Se_6I_2)[AsF_6]_2 \bullet 2SO_2(s) \rightarrow (Se_6I_2)[AsF_6]_2(s) + 2SO_2(l) \quad (3)$$

$$(Se_6I_2)[AsF_6]_2 \bullet 2SO_2(s) \rightarrow (Se_6I_2)[AsF_6]_2(s) + 2SO_2(g) \quad (4)$$

$$(Se_8)[AsF_6]_2 \bullet \tfrac{1}{3}SO_2\,(s) \rightarrow (Se_8)[AsF_6]_2\,(s) + \tfrac{1}{3}\,SO_2(l) \quad (5)$$

$$(Se_8)[AsF_6]_2 \bullet \tfrac{1}{3}SO_2\,(s) \rightarrow (Se_8)[AsF_6]_2\,(s) + \tfrac{1}{3}\,SO_2(g) \quad (6)$$

In these reactions SO_2 is lost either in liquid or gaseous form from the solvate. The discussion has to be carried out in the absence of any thermodynamic data ($\Delta_f H^o$ etc.) either for the above solvates *or* for their parent salts. The innovative step that opens up the way to providing data for non–aqueous materials is the use of the Thermodynamic Solvate Difference Rule.[58] This rule was devised from a study of the patterns exhibited within standard thermodynamic data for hydrated salts (and other non–aqueous solvates).[58] The rule expresses the observed fact that the *differences* in standard thermodynamic properties, P (= $\Delta_f H^o$, $\Delta_f G^o$ and S^o etc.) between a solvated salt and its unsolvated parent, in a solvent like SO_2, is equal to a constant, $\Theta_P(SO_2,s–s)$ multiplied by n, the number of solvate molecules, for the solvates of interest, in the analytical forms:

$$P\{(Se_6I_2)[AsF_6]_2.2SO_2,s\} - P\{(Se_6I_2)[AsF_6]_2,s\} \approx 2\,\Theta_P(SO_2,s–s) \quad (7)$$

$$P\{(Se_8)[AsF_6]_2.\,\tfrac{1}{3}SO_2,s\} - P\{(Se_8)[AsF_6]_2,s\} \approx \tfrac{1}{3}\,\Theta_P(SO_2,s–s) \quad (8)$$

Details of the application of this rule to determine the thermodynamics of equations (3)–(6), are given in the Supporting Information. $\Theta_P(SO_2,s–s)$, as well as being constant, is independent of the nature of the chemical.

Results and Discussion

General. When $(Se_6I_2)[AsF_6]_2$ is dissolved in SO_2(l), it dissociates forming several cationic species. The ^{77}Se NMR spectrum of the equilibrium solution of the ^{77}Se–enriched sample is shown in Figure 3. The assignment of the resonances and the identification of cationic species are based on the following considerations: comparison of the NMR spectra of ^{77}Se–enriched and natural–abundance samples, PS–DQF ^{77}Se–^{77}Se COSY, homonuclear ^{77}Se–^{77}Se decoupling experiments, spectral simulations, consideration of the trends in chemical shifts, and consideration of selenium, iodine, and charge balances.

Since natural–abundance selenium contains only 7.58 % of ^{77}Se, the coupling information in natural–abundance spectra is only seen as an appearance of small satellites that often get lost in the background. Consequently, the comparison of the ^{77}Se NMR spectrum of the enriched sample with that involving natural–abundance selenium can be used to establish the number of discrete resonances that give rise to the coupling multiplets. For instance, most of the multiplets in the enriched spectrum in Figure 3 appear as discrete singlets in the natural–abundance spectrum. In some cases two resonances overlap. In these cases the observed resonances in the natural–abundance spectrum have been shown as inserts in Figure 3. For instance, a complicated coupling pattern can be observed for the resonance *11*. The appropriate portion of the natural–abundance spectrum shown in the insert demonstrates that the complete coupling multiplet in the enriched spectrum arises from two close–lying resonances marked *11a* and *11b*. Similarly, there is a weak multiplet *13* that is virtually

hidden beneath the strong resonance *12*. Both resonances can be observed as singlets in the natural–abundance spectrum. This comparative information in Figure 3 has been used to establish the presence of 32 resonances in the spectrum. In addition, two very weak resonances at 1103 and 774 ppm could be observed in the natural abundance spectrum. In the ^{77}Se–enriched spectrum, the latter is observed but the former is obscured by resonances *20* and *21*.

PS–DQF ^{77}Se–^{77}Se COSY spectrum shown in Figure 4 has been used to establish that the observed 32 resonances arise from 11 different cationic species. This conclusion was verified by the homonuclear ^{77}Se–^{77}Se decoupling experiments.

Previously identified cations. The chemical shifts that have previously been reported for 1,4–$Se_6I_2^{2+}$ (**1**),[21] SeI_3^+ (**2**),[21] 1,1,4,4–$Se_4I_4^{2+}$ (**3**),[21] and Se_4^{2+} (**4**),[82] Se_8^{2+} (**5**),[83] and Se_{10}^{2+} (**6**) [83] could be identified in the spectrum of the dissociation products and are indicated in Figure 3.[84] Their chemical shifts and coupling information, as well as calculated chemical shifts have been presented in Table 3.

SeI_3^+. The PBE0/(SDB) –cc–pVTZ optimized structure of the smallest selenium–iodine cation SeI_3^+ (**2**) is shown in Figure 5 together with the natural atomic charges and the order of the Se–I bond. Its ^{77}Se resonance appears as a singlet at 830 ppm in agreement with the chemical shift reported previously.[21] The structure and spectroscopic properties of SeI_3^+ have been studied in our theoretical account [51] along with several other selenium species in order to estimate the ability of the quantum chemical calculations to produce reliable predictions for the selenium species. The calculated structures and vibrational frequencies were found to be in good agreement with experimental values already at non–relativistic (nr) level. The chemical shifts of selenium species containing atoms lighter than selenium calculated at nr level were also in a fair agreement with the experimental chemical shifts. Similar observations have also been reported in other studies.[49] By contrast, the agreement with the nr chemical

shifts and the experimental chemical shifts for selenium–iodine species was poor (cf. SeI_3^+ calc. nr 1362 ppm [51] vs. exp. 830 ppm). The relativistic ZORA calculations were shown to improve the agreement over the non–relativistic calculation for the selenium iodine species (SeI_3^+ calc. ZORA 1294 ppm) [51] but still fail to give the accuracy required for unambiguous identification of selenium iodine species.

The solvent effects have been shown to cause large changes in the chemical shifts especially for heavier elements.[76,139] A proper description of the solvent effects on chemical shifts is considered to require the explicit inclusion of the first solvation shell alongside with the continuum solvation effects.[87]

Even though it is not possible to account for the full first solvation shell due to the computational cost, it can be shown that by adding explicit SO_2 molecules to the calculations and using COSMO model to account for the bulk solvent effects the agreement between calculated and experimental chemical shifts can be improved. The effect of adding SO_2 molecules to the calculation of the ^{77}Se chemical shift of SeI_3^+ is illustrated in Figure 6. The cation–solvent molecule clusters have been optimized starting from structures where SO_2 molecules are located near the atoms to which they are expected to coordinate. Compared to the vacuum ^{77}Se chemical shift [see Figure 6(a)], coordination of the selenium atom with a SO_2 molecule appears to move the chemical shift slightly to downfield thus moving the calculated chemical shift away from the experimental chemical shift [See Figure 6(b)]. By contrast, coordination of iodine atom with a SO_2 molecule moves the ^{77}Se chemical shift significantly upfield and closer to the experimental chemical shift [Figure 6(c)]. Addition of more SO_2 atoms to coordinate to the remaining iodine atoms moves the ^{77}Se chemical shift even closer to the experimental chemical shift. The best calculated result 1006 ppm is obtained with three SO_2 molecules coordinating all iodine atoms [Figure 6(d)]. Addition of fourth SO_2 molecule to coordinate to the selenium atom moves the ^{77}Se chemical shift

downfield by 62 ppm [Figure 6(e)]. Addition of even more SO_2 molecules does not seem to improve the calculated chemical shift further (e.g. ^{77}Se chemical shift calculated with 9 SO_2 molecules is 1004 ppm; See Supporting Information). The remaining difference between the experimental and calculated chemical shifts of SeI_3^+ can be attributed to the approximate way the explicit solvent effects have been included and the combined heavy atom effect of three iodine atoms that may be underestimated by the ZORA approximation. Similar underestimation of shielding by ZORA calculations was apparent in the recently reported ^{119}Sn chemical shifts of tin iodides where three of the four iodine atoms were bound to the tin atom, while the agreement between the calculated and experimental ^{119}Sn chemical shifts for the species containing fewer iodine atoms was much better.[88]

Following the observations made for calculated ^{77}Se chemical shifts of SeI_3^+, the chemical shifts of other selenium–iodine cations were calculated by using explicit solvent molecules to coordinate to all iodine atoms. For the larger selenium–iodine cations and Se_4^{2+} and Se_8^{2+} additional SO_2 molecules were included in the calculations to coordinate also to selenium atoms in order to have a more uniform description of the solvent surroundings. These additional SO_2 molecules were placed around the cations in an even manner prior to optimization of the cluster structures. The coordinates of the optimized cation–solvent molecule clusters have been included in Supporting Information.

1,4–$Se_6I_2^{2+}$. The spectral simulation of the resonances at 1313 and 478 ppm that are assigned to 1,4–$Se_6I_2^{2+}$ was carried out by considering all possible isotopomers. 1,4–$Se_6I_2^{2+}$ is a six–spin AA'MM'M"M"' system, if all selenium atom positions are simultaneously occupied by the ^{77}Se nucleus (A and A' denote the two selenium atoms bound to iodine, and M, M', M", and M"' denote the four selenium atoms not bound to iodine). At the 92 % level of enrichment the probability of this fully enriched isotopomer is 58 %. The other major isotopomers that have an effect on the observed spectrum are the five–spin systems

AMM'M"M"' (2 isotopomers; probability 10 %), AA'MM'M" (4 isotopomers, probability 20 %), and the four–spin system AMM'M" (8 isotopomers, probability 3 %). The missing selenium–atom positions are occupied by nuclei of other selenium isotopes that are NMR inactive. The different isotopomers shown in Figure 7 each yielded reasonable coupling constants (see Table 3), and thus verified their identities. The appearance of the simulated spectra as a sum of the coupling patterns due to different isotopomers also compares well with the coupling patterns of the experimental resonances, as shown in Figure 7.

The spectral simulation allows for two conformations of $Se_6I_2^{2+}$ [*endo,endo* (**1₁**) and *exo,exo* (**1₂**)] [89] that have been considered in the literature.[22] The **1₁** conformation corresponds to the solid state structure of $Se_6I_2^{2+}$ presented in Figure 1 and the **1₂** conformation to a structure where the exocyclic iodine atoms adopt a less hindered positions pointing away from the ring. The **1₂** conformation has a similar structure to that of $As_2Se_6^{2-}$.[90] The *endo,endo* (**1₁**) and *exo,exo* (**1₂**) conformations were optimized for $Se_6I_2^{2+}$ using D_{2h} symmetry. The optimized structures are presented in Figure 8. Both conformations are very close to each other in energy. In the gas phase, the **1₂** conformation is slightly lower in energy (3.5 kJ/mol) than the **1₁** conformation, while in SO_2 solution the **1₁** conformation is estimated to be the more stable (15.7 kJ/mol).[91] However, the energy differences between different conformations are well within the error limits of the computational methods and do not provide conclusive evidence which conformation is the preferred one in the SO_2 solution. On the other hand, the calculated chemical shifts of the **1₁** conformation [(Se1 416/498 ppm, Se2 1407/1319 ppm (vacuum/solvent); see Table 3)] agree much better with the experimental chemical shifts than the chemical shifts of the **1₂** conformation (Se1 688/674 ppm, Se2 1778/1584 ppm) and confirm that the 1,4–$Se_6I_2^{2+}$ also retains its solid state structure in SO_2 solution.

Structure and Bonding in 1,4–$Se_6I_2^{2+}$. Most of the calculated structural parameters for the **1₁** conformation shown in Figure 8 are in good agreement with those from the

experimental crystal structure shown in Figure 1. Only the Se2···I contacts are predicted to be significantly too long by the DFT optimization. This can be accounted for either by the failure of the DFT functional to model the dispersion forces properly in case of weak interactions,[92] or by crystal packing effects in the experimental solid state structure that are missing in the calculations.

The strong selenium–selenium bond alternation observed in the experimental structure of $Se_6I_2^{2+}$ has previously been attributed to the delocalization of the positive charge from the tricoordinate selenium atoms and is well reproduced by the calculated $\mathbf{1}_1$ structure. This bond alternation caused by the charge delocalization has been described by five resonance structures shown in Figure 2.[22b] The resonance structure **i** represents the all σ bonded parent Lewis structure for $Se_6I_2^{2+}$, where the positive charges are localized on the trivalent Se1 atoms. The resonance structures **ii** and **iii** show the weakening of Se1–Se2 and strengthening of Se2–Se2 bonds accompanied by delocalization of the positive charge to Se2 atoms, and the resonance structures **iv** and **v** show the charge delocalization from Se1 atoms to iodine atoms which leads to the strengthening of the Se1–I bonds. Similar considerations have been derived to explain, qualitatively, the observed bond alternations in a variety of other polychalcogen cations (e.g. S_7I^+).[93]

The calculated relative bond orders and natural atomic charges confirm the observed bond alternation and the expected delocalization of the positive charge [see Figure 8(a)]. Similar even distribution of positive charges between selenium and iodine has also been calculated for SeI_3^+(**2**) (see Figure 5). A rough estimate of the extent to which charge delocalization stabilizes $Se_6I_2^{2+}$ was calculated to be –29.6 kJ/mol, which is the [CCSD(T)/(SDB)–cc–pVTZ] energy difference between a partially optimized structure with Se–Se (2.326 Å) and Se–I (2.518 Å) constrained to approximate single bond lengths and that of the fully optimized *endo, endo* conformation.

The Se1–Se2 bonds in 1,4–$Se_6I_2^{2+}$ (**1₁**) show bond orders of only 0.7, while those of the Se2–Se2 bonds are well above a single bond (1.2). The NBO analysis effectively describes the charge delocalization by p^2[Se2] → σ*[Se1–Se2] and p^2[I] → σ*[Se1–Se2] electron transfers (see Figure 9) in accordance with the resonance structure description above (see Supporting Information for NBO results). The p^2[Se2] → σ*[Se1–Se2] hyperconjugation increases the occupancy of the σ*[Se1–Se2] orbital weakening the Se1–Se2 b,,,ond and at the same time forms a weak π type interaction between two Se2 atoms increasing the Se2–Se2 bond order. Thus this analysis quantitatively confirms that $Se_6I_2^{2+}$, like many related species, e.g. $S_2I_4^{2+}$, S_7I^+, M_4^{2+} (M = S, Se, Te), form stable npπ–npπ (n ≥ 3) bonds at the expense of σ bonds, as a consequence of charge delocalization, as previously proposed.[54,55,93,94] The p^2[I] → σ*[Se1–Se2] hyperconjugation further weakens the Se1–Se2 bond while forming a weak 5pπ–4pπ bond between iodine and Se1 atoms and increasing the Se1–I bond order. The p^2[Se2] and p^2[I] NBOs are σ* anti–bonding with respect to each other, as shown in Figure 9. The decrease in the occupation of these two NBOs could explain the existence of a weak bonding interaction between Se2 and I atoms as previously proposed to account for the cluster like geometry of $Se_6I_2^{2+}$ and related cations. [22,45,54,93,94] The AIM analysis shows that there are bond critical points between Se2 and I atoms with a small bond order 0.2 which is consistent with a weak bonding interaction. However the lower CCSD(T)/(SDB)–cc–pVTZ energy of the less sterically hindered **1₂** conformation suggest that the weak Se2···I bonding interaction may not be strong enough by itself to make the **1₁** conformation the minimum structure and that environmental effects may play a role in determining the minimum structure in the solid state.

1,1,4,4–$Se_4I_4^{2+}$. The spectral simulation of the two resonances at 1548 and 978 ppm assigned to 1,1,4,4–$Se_4I_4^{2+}$ is shown in Figure 10. At 92 % level of enrichment, the probability for 1,1,4,4–$Se_4I_4^{2+}$ to be a fully enriched four–spin system AA'MM' is 73 %. The

other major contributors to the observed spectrum are the three–spin systems AA'M (2 isotopomers; probability 12 %) and AMM' (2 isotopomers; probability 12 %). The simulated spectra agree well with the observed spectra (see Figure 10) and the simulation yields reasonable coupling constants given in Table 3 confirming the assignment.

A solid containing 1,1,4,4–$Se_4I_4^{2+}$ has not yet been isolated. Therefore its structure has not yet been experimentally determined. All attempts to crystallize solutions of $(Se_4I_4)[AsF_6]_2$ made by the reaction of Se_4^{2+} and I_2 in SO_2 solution, containing $Se_4I_4^{2+}$ and its equilibrium products Se_8^{2+} and SeI_3^+, led to the isolation of either $(SeI_3)[AsF_6](s)$ or $(Se_8)[AsF_6]_2$ (s).[21]

$$3\ Se_4^{2+}(solv) + 6\ I_2(s) \rightarrow 3\ Se_4I_4^{2+}(solv) \leftrightharpoons Se_8^{2+}(solv) + 4\ SeI_3^+(solv) \qquad (15)$$

The observation of only two resonances for 1,1,4,4–$Se_4I_4^{2+}$ is consistent with the $I_2Se^+SeSeSe^+I_2$ chain structure having two–fold symmetry. All attempts to optimize different conformations for 1,1,4,4–$Se_4I_4^{2+}$ (**3**) resulted in only one minimum structure shown in Figure 11. The low field vacuum shift calculated for the minimum structure is in good agreement with the experimental resonance (see Table 3), but the calculated high field shift for the selenium atoms bonded to two iodine atoms is predicted higher than the observed resonance by some 200 ppm. The explicit solvent calculation moves both calculated resonances to higher field and improves the overall agreement with the experimental data. Although the agreement with the experimental and calculated chemical shifts is not as good as for 1,4–$Se_6I_2^{2+}$ it can be considered to be sufficiently good to confirm the assignment of the resonances at 1548 and 978 ppm to 1,1,4,4–$Se_4I_4^{2+}$.

Structure and Bonding in 1,1,4,4–$Se_4I_4^{2+}$. The optimized structure of 1,1,4,4–$Se_4I_4^{2+}$ (**3**) is a chain that minimizes the steric repulsion. It does not exhibit the long Se2···I contacts that could be expected on the basis of the structure of 1,4–$Se_6I_2^{2+}$.[95] The bond alternation that was

observed in 1,4–$Se_6I_2^{2+}$ on the other hand is also present in the selenium chain of 1,1,4,4–$Se_4I_4^{2+}$ (see Figure 11). The middle Se2–Se2 bond is considerably shorter (bond order 1.2) than the terminal Se1–Se2 bonds (bond order 0.7). The natural charges indicate similar kinds of charge distributions between the selenium atoms and the iodine atoms in both 1,1,4,4–$Se_4I_4^{2+}$ and 1,4–$Se_6I_2^{2+}$.

The NBO analysis describes the positive charge delocalization from the tri–coordinated Se1 atoms to Se2 and iodine atoms by p^2[Se2] $\rightarrow$ σ^*[Se1–Se2] and p^2[I] $\rightarrow$ σ^*[Se1–Se2] hyperconjugation (see insert in Figure 11). The p^2[Se2] $\rightarrow$ σ^*[Se1–Se2] electron transfer weakens the Se1–Se2 bonds compared to the purely σ bonded Lewis structure. At the same time, the weak π bond formation between the Se2 atoms increases the Se2–Se2 bond order from unity. In a similar fashion, the p^2[I] $\rightarrow$ σ^*[Se1–Se2] hyperconjugation renders the Se1–I bonds some π character and weakens the Se1–Se2 bonds even further. A partially optimized 1,1,4,4–$Se_4I_4^{2+}$ structure with Se–Se and Se–I bonds constrained to single bonds was calculated to be only +3.9 kJ/mol higher in energy at CCSD(T)/(SDB)–cc–pVTZ level than the minimum structure. This indicates that charge delocalization does not play as large a role in the structure of 1,1,4,4–$Se_4I_4^{2+}$, as it does in the structure of 1,4–$Se_6I_2^{2+}$.

Se_4^{2+}. The singlet resonance at 1922 ppm can be assigned to Se_4^{2+} (**4**) by comparison to the value 1936 ppm reported in literature.[82] The chemical shift of Se_4^{2+} was recently calculated by Tuononen *et al.*[85] It turned out to be necessary to use multiconfiguration methods to properly account for the electron correlation in Se_4^{2+} and to accurately predict its spectroscopic properties with *ab initio* calculations (cf. CASPT2 1893 ppm vs. exp. 1922 ppm). Pure DFT calculations were also shown to give good ^{77}Se NMR chemical shifts for Se_4^{2+} (BPW91 1941 ppm) and related four–membered ring cations.[85] In accordance with previous results, the present pure DFT rPBE chemical shift calculations yield the ^{77}Se chemical shift of 1925 ppm for Se_4^{2+} that agrees well with the experimental chemical shift.

The explicit solvent calculation moves the chemical shift of Se_4^{2+} slightly to a lower field but does not induce a significant change in the chemical shift.

Se_8^{2+}. The presence of Se_8^{2+} can be inferred by five resonances at 1970, 1521, 1196, 1071, and 1046 ppm that show the same intensity ratio (2:2:1:2:1) and coupling patterns, as reported earlier by Burns *et al.*[83] (see Table 3). The optimized structure of Se_8^{2+} (**5**) is presented in Figure 12(a) and compared to the experimental structural parameters [96] that are in good agreement with the computed values. The bonding in Se_8^{2+} has been discussed in detail by Cameron *et al.*[45]

The calculated chemical shifts of Se_8^{2+} are shown in Table 3. The computed chemical shifts show a good agreement with the observed chemical shifts when solvent effects are taken into account. Our assignment, however, is somewhat different from that given earlier.[83] Their assignment was based on spectral simulation assuming that the atoms at *exo* end of the cation [see Figure 12(a)] are less shielded than the atoms at the *endo* end of the cation [*i.e.* 1970 ppm ≡ Se(3), 1521 ppm ≡ Se(4), 1196 ppm ≡ Se(5), 1071 ppm ≡ Se(2), and 1046 ppm ≡ Se(1)]. As shown in Table 3, our calculated chemical shifts show an opposite trend. Compared to the assignment of Burns *et al.*,[83] our assignment leads to spin–spin coupling constants that show slightly less reasonable values {cf. original assignment *J*[Se(1)–Se(4)] = 0 Hz and *J*[Se(2)–Se(5)] = ±18.4 Hz; our reversed assignment J[Se(1)–Se(4)] = ±18.4 Hz and J[Se(2)–Se(5)] = 0}. On the other hand, if the earlier assignments are retained then the calculated chemical shifts show a large discrepancy with the experimental chemical shifts thus justifying the reconsideration of the assignment.

Se_{10}^{2+}. The two very weak resonances at 1103 and 774 ppm are assigned to Se_{10}^{2+}.[83] The computed structure of Se_{10}^{2+} (**6**) is presented and compared to the crystal structure parameters in Figure 12(b).[97] The optimized structural parameters of Se_{10}^{2+} are close to the experimental

structure.[98] The optimized structure of S_{10}^{2+} was recently reported and found to have the same structural features as the experimental structure of Se_{10}^{2+}.[47]

The comparison between calculated and experimental chemical shifts has not been attempted for Se_{10}^{2+}, because the cation is fluxional in the SO_2 solution exhibiting only two resonances.[83] The fluxionality prevents a simple comparison between the observed chemical shifts and those calculated for a fixed structure. Furthermore, Burns *et al.*[98] concluded that Se_{10}^{2+} will not retain its solid state structure in solution based on the considerable difference between the electronic spectra of solid $(Se_{10})[AsF_6]_2$, and that given on dissolution in liquid SO_2.

The Remaining 22 Resonances. A tentative assignment of the remaining 22 unknown resonances has been carried out by PS–DQF ^{77}Se–^{77}Se COSY, homonuclear ^{77}Se–^{77}Se decoupling experiments, as well as by spectral simulation that together yield information on the number of species and their spin systems. The ^{77}Se–^{77}Se COSY spectrum of the ^{77}Se–enriched $(Se_6I_2)[AsF_6]_2$ is shown in Figure 4. The correlations could be used to distribute the resonances into five groups **A**–**E** (see Table 4) and the spectral simulations were utilized to establish the spin systems they represent.

Spin Systems. The two resonances of equal intensity at 1486 and 1219 ppm (resonances *8* and *14*) also show coupling connectivity according to ^{77}Se–^{77}Se COSY and homonuclear decoupling experiments and therefore form the Group **A**. Both resonances appear as very broad doublets (see Figure 13). The coupling constant is given in Table 4.

Group **B** consists of three resonances *17*, *20*, and *21* at 1181, 1096, 1094 ppm (relative intensities 1:1:1). ^{77}Se–^{77}Se COSY and homonuclear decoupling experiments indicate coupling correlation from the resonance *17* to the resonances *20*, and *21*, and from the resonance *20* to the resonance *21*. This set of three resonances represents a six–spin system with three symmetry–related pairs of ^{77}Se nuclei. The observed and simulated coupling

patterns of these three resonances are shown in Figure 14 and the coupling constants in Table 4. A very good agreement between the calculated and observed coupling patterns is demonstrated in Figure 14.

There are six resonances of equal intensity forming the Group **C** at 1597, 1351, 1350, 1170, 1007, 873 ppm (resonances *5*, *11a*, *11b*, *18*, *26*, and *30*). The coupling correlation is observed between the resonances *5*, *11a,b*, and *26*, as well as between *11a,b*, *18*, and *30*. The observed and calculated coupling patterns are consistent with each other and are shown in Figure 15 and the coupling constants in Table 4.

Four observed resonances at 1149, 1064, 1044, and 998 ppm (relative intensities 2:2:1:2) form group **D**. The ^{77}Se–^{77}Se COSY spectrum showed correlation from the resonance *19* to the resonance *27*, and from the resonance *23* to the resonances *25*, and *27*. The resonances could be simulated in terms of a seven–spin system. The coupling constants are shown in Table 4. The observed and calculated coupling patterns again agree well with each other (see Figure 16).

Group **E** consists of seven resonances of equal intensity at 1791, 1637, 1419, 1374, 1308, 1200 and 956 ppm (resonances *3*, *4*, *9*, *10*, *13*, *15*, and *29*, respectively). The resonances *3*, *4*, and *10* show coupling correlation, as do resonances *4* and *13*, and *9*, *13*, *15*, and *29*. The spectral simulation based on this information yielded the coupling constants shown in Table 4. A very good agreement between the calculated and observed coupling patterns is demonstrated in Figure 17.

Tentative Identification of the Cationic Species. Additional information is required to establish the chemical identities of the cations that the spin systems **A**–**E** represent. The calculated ZORA rPBE / QZ4P chemical shifts, the iodine, selenium, and charge balances in the course of the dissociation of 1,4–$Se_6I_2^{2+}$, as well as the trends in the chemical shifts deduced from those of the known species have been considered to facilitate the assignment of

the five resonance groups in the ^{77}Se spectrum. An internally consistent assignment is proposed in the following. It should be noted, however, that the presented assignment does not completely rule out the possibility that the spin–systems could also represent other cations. Furthermore, ^{77}Se NMR spectroscopy cannot be directly used to infer the presence or absence of homonuclear iodine cations.

Group A. The two weak resonances in this group are assigned to 1,1,2–$Se_2I_3^+$ (**7**). The optimized structure is presented in Figure 18(a). The ZORA rPBE / QZ4P NMR chemical shifts for 1,1,2–$Se_2I_3^+$ are in approximate agreement with the group **A** resonances giving support for this assignment (see Table 4).[100]

The structure **7** contains a dicoordinate, formally neutral Se atom [Se2; see Figure 18(a)] bound to iodine. Stable solids containing dicoordinate Se–I are only known for RSeI where R is a very bulky group e.g. 2,4,6–*t*$Bu_3C_6H_2$,[101] which kinetically hinders I_2 elimination and thermodynamically disfavors the products by introducing strain in the Se–Se bond of the resulting RSe–SeR and thus weakening the bond. The relative weakness of the bonds between neutral selenium and iodine atoms has been related to the similarity of their electronegativities. It appears that a significant amount of positive charge is transferred from the formally positively charged Se1 to Se2 and also to the iodine atom bound to Se2 [see Figure 18(a)]. The positive charge transfer from Se2 to iodine atom strengthens the Se2–I bond by giving it π character in a similar manner to the Se–I bonds in $Se_6I_2^{2+}$. The increase in π character results in a relatively short Se2–I bond and a high relative Mayer bond order of 1.2, which surprisingly is calculated to be even higher than those for the two Se1–I bonds.[102]

Further support for the plausibility of finding 1,1,2–$Se_2I_3^+$ in SO_2 solution is given by the calculations reported in our preliminary theoretical account, which confirmed the experimental NMR results of Gopal and Milne [10] who identified SeI_2 and Se_2I_2 in CS_2 solution. This indicates that even though bonds between neutral selenium and iodine atoms

are unstable in the solid state with respect to I_2 elimination,[2] the same is not necessarily true in solution where the overall energetics are governed by differences in the energy of the solvated cations and that of iodine in solution.

Group B. The equal intensities and coupling constants of the three resonances of group **B** are consistent with a six–membered selenium chain structure 1,1,6,6–$Se_6I_4^{2+}$ (**8**). The geometry optimization yielded three local minima for the 1,1,6,6–$Se_6I_4^{2+}$ chain corresponding to different orientations of the terminal SeI_2 units with respect to the four central selenium atoms. The optimized structures are shown in Figure 18(b).

The asymmetric structure $\mathbf{8_1}$ has the lowest total energy in SO_2 solution. The other two conformations $\mathbf{8_2}$ and $\mathbf{8_3}$ both show C_2 symmetry and were found to be 0.9 and 5.7 kJ mol^{-1} less stable, respectively. Thus, as energy differences are small, it is likely that there is rapid interconversion between the different conformations rendering them indistinguishable on the NMR time scale. Therefore, the experimental chemical shifts are compared with the computed chemical shifts that are calculated as averages of chemical shifts of individual conformations.[99] The experimental and calculated average chemical shifts are compared in Table 4. The calculated chemical shifts for 1,1,6,6–$Se_6I_4^{2+}$ are not inconsistent with the experimental chemical shifts when six explicit SO_2 solvent molecules are used in the computation, thus giving confidence in the assignment.[103]

The calculated structures of 1,1,6,6–$Se_6I_4^{2+}$ show an elongated chain structure in a similar fashion to 1,1,4,4–$Se_4I_4^{2+}$. The structures again maximize the bond alternation resulting from the charge delocalization from formally positively charged tri–coordinated selenium atoms to the chain.

Group C. The six resonances of group **C** with equal intensities are expected to result from an asymmetrical six–membered selenium chain structure and the high field shifts at 1007 and 873 ppm are expected to be due to selenium atoms bonded to iodine. 1,1,6–$Se_6I_3^{+}$

(**9**) was considered to be a reasonable candidate for the asymmetrical selenium chain structure.

The optimization of a 1,1,6–$Se_6I_3^+$ chain structure lead to two local minima. They are presented in Figure 18(c). The conformation **9₂** lies 4.0 kJ mol^{-1} higher in energy than the conformation **9₁**. As in the case of 1,1,6,6–$Se_6I_4^{2+}$, it is probable that both conformations **9₁** and **9₂** are in equilibrium in SO_2 solution and contribute to the observed chemical shifts. Therefore, the average from both conformations is considered a reasonable approximation, when computed chemical shifts are compared to the observed chemical shifts (see Table 4).[99,103] We note that $Se_6I_3^+$ was the only cation for which the experimental trend of the observed chemical shifts of group **C** was reproduced.[104] The observed coupling information of the six resonances in this group is also consistent with 1,1,6–$Se_6I_3^+$.

The conformations **9₁** and **9₂** both show elongated chain structures similar to those in 1,1,6,6–$Se_6I_4^{2+}$ [see Figures 18(b) and 18(c)]. 1,1,6–$Se_6I_3^+$ does not show similar bond alternation to 1,1,6,6–$Se_6I_4^{2+}$, because the dicoordinate Se–I moiety does not give rise to charge delocalization. As a result, while the Se1–Se2 bond at the I_2Se^+ end of the cation is long and the Se2–Se3 is short, the Se3–Se4 and Se4–Se5 bonds are normal single bonds. The Se5–Se6 bond is slightly shorter than the single bond.

It can be expected that because of the dicoordinate Se–I, 1,1,6–$Se_6I_3^+$ is less stable than 1,1,6,6–$Se_6I_4^{2+}$. However, since the existence of dicoordinate Se–I bonds has been reported in solution,[105] it is reasonable to expect that 1,1,6–$Se_6I_3^+$ can exist in SO_2 solution. On the other hand, it is unlikely that the structures like $ISe(Se)_nSe^+I_2$ can be isolated in the solid phase.

Group D. The observed resonances correspond to a seven–spin ABB'CC'DD' system and span a rather narrow chemical shift range (see Figure 3). The resonances are assigned to cyclic Se_7I^+ (**10**) that is assumed to have a structure that is analogous to the well–known

S_7I^+.[93] Even though Se_7I^+ has not been identified and characterized in the solid state it is reasonable to expect that it will exist in SO_2 solution.

The four optimized structures of Se_7I^+ that are very close in energy are shown in Figure 19 together with their relative free energies in SO_2 solution. The global minimum shows a conformation **10₁** with a very similar geometry to that observed for S_7I^+.[93,94] The conformation **10₂** shows the iodine atom bonded to one of the middle selenium atoms in the approximately coplanar Se_4 fragment and is directed away from the seven–membered ring. It lies only 1.9 kJ mol^{-1} above the conformation **10₁**. The conformation **10₃** has a boat conformation and lies 8.9 kJ mol^{-1} above **10₁**. The conformation of highest energy **10₄** is rather similar to the conformation **10₁**, but the iodine atom is turned away from the ring. It lies 12.2 kJ mol^{-1} above **10₁**.

The DFT calculations indicate that the Se_7I^+ cation is fluxional and undergoes facile pseudorotation in the same fashion as has earlier been observed for the electrically neutral seven–membered sulfur and selenium ring molecules (see Ref. 106, for a review). Because of the pseudorotation, the chemical environment and therefore the chemical shift of each selenium atom in Se_7I^+ is changing rapidly at the NMR time scale. The DFT calculations indeed indicate that the calculated chemical shifts of the corresponding selenium atoms vary significantly from conformation to conformation (**10₁ 10₂**, **10₃**, and **10₄**). Therefore no agreement with the observed chemical shifts from any given fixed optimized structure can be expected (see Ref. 99, for the calculated chemical shifts of individual conformations **10₁**–**10₄**). Futhermore, no individual structure in Figure 19 displays the expected ABB'CC'DD' spin system. The cation and the calculated spin system show a virtual two–fold symmetry and the observed when pseudorotation is taken into account. The average values of the corresponding chemical shifts of the different conformations also provide a better estimate of the observed chemical shifts (see Table 4). The agreement is, as expected, approximate, since it is likely

that there are several pseudorotation intermediates between the different conformations and their chemical shifts would also play a significant role in the observed average chemical shifts.[103]

Group E. The seven resonances with equal intensities imply seven independent selenium atoms. One reasonable candidate is $(4–Se_7I)_2I^{3+}$ (**11**) for which a sulfur analogue is known in the solid state.[94] The optimized geometry of the cation is shown in Figure 20. The conformations of the two Se_7I rings are not quite identical with those observed in the crystal structure of $\{(S_7I)_2I\}[SbF_6]_3$, but taking into account that the seven–membered rings in **11** probably show several conformations with virtually identical energy, it is conceivable that the crystal packing effects are important in determining the solid state conformations.

$(4–Se_7I)_2I^{3+}$ is expected to show seven ^{77}Se resonances assuming that in solution the two Se_7I rings are equivalent and that coupling information is not carried across the bridging quadrupolar iodine. The computed ^{77}Se chemical shifts are consistent with the observed resonances and coupling information (see Table 4). We were not able to carry out explicit solvent computations for $(4–Se_7I)_2I^{3+}$, since calculations that would have included enough explicit solvent molecules to improve the agreement over vacuum values were not possible with the computational resources available.

Trends in Chemical Shifts and Coupling Constants. The chemical shifts of the cations that have been proposed to account for the 22 unknown resonances are summarized in Figure 21. It can be seen that the qualitative trends in the chemical shifts are self–consistent and provide support for the assignment. Generally, the resonances of the selenium atoms that are bonded to iodine expectedly lie at higher field than those of other selenium atoms, though there seem to be exceptions, in particular when the species are expected to be fluxional.

We note that for most part, the coupling constants show a trend that is consistent with the expected bond length alternations within the cations (see Figure 22 for some examples).

However, the coupling between the nuclei in these species is not only dependent on Fermi contact term, but through–space coupling involving lone–pair electrons also has an effect on the magnitude of coupling constants.

Selenium, Iodine, and Charge Balance. Further verification for the identification of the cations can be obtained by considering the iodine, selenium, and charge balances during the dissociation (see Table 5). Let there be initially 100 mol of 1,4–$Se_6I_2^{2+}$ implying 600 mol of selenium, 200 mol of iodine, and 200 mol of charge. The spectral assignment and integrated intensities of the resonances in the equilibrium mixture enable the calculation of the relative abundances of the cationic species and therefore also the final distribution of selenium and iodine.[107] It can be seen from Table 5 that within the accuracy of the experiment, the current assignment accounts well for the selenium, iodine, and charge balances.[108] There are 600 moles of selenium in the initial 1,4–$Se_6I_2^{2+}$ and 624(31) moles selenium in the equilibrium solution. Of 200 moles of initial iodine, there are 213(11) moles in the equilibrium solution and of 200 moles of charge, there are 188(9) moles in the final solution.[109]

The Reversible Equilibrium of $(Se_6I_2)[AsF_6]_2{\cdot}2SO_2$ in Liquid SO_2 Solution. In solution 1,4–$Se_6I_2^{2+}$ is in equilibrium with Se_n^{2+}(n = 4, 8, 10), SeI_3^+, 1,1,4,4–$Se_4I_4^{2+}$, 1,1,6,6–$Se_6I_4^{2+}$, Se_7I^+, $[(4–Se_7I)_3I]_3^+$, 1,1,6–$Se_6I_3^+$ and 1,1,2–$Se_2I_3^+$, connected *via* equations (1), (2), and numerous other equilibria that can be envisaged. We note Se_{10}^{2+} has never been observed in the presence of Se_4^{2+}, with which it is expected to react to give Se_8^{2+}.[44] However all Se_n^{2+} (n= 4, 8, 10) are detected in solutions of $Se_6I_2^{2+}$. Presumably the overall energy balance of the complex equilibria of which they are a part permits their presence, as well as other otherwise unstable species, e.g. 1,1,6–$Se_6I_3^+$ and 1,1,2–$Se_2I_3^+$.

Homogeneous crystals of $(Se_6I_2)[AsF_6]_2{\cdot}2SO_2$ can be recovered by cooling the solution to –80°C for 10 minutes and then leaving it to stand at room temperature for one day.[22b,c]. The equilibrium solution can be regenerated on sonification of the solid in SO_2(l). As far as we are

aware such a complex reversible equilibrium involving ionic species is without precedent, although it is reminiscent of the equilibrium mixture of liquid sulfur just above the melting point containing S_8 together with numerous S_x ($x \geq 6$). S_8 is regenerated upon solidification.[110]

Thermodynamics. In this paper, we provide a thorough treatment of the thermodynamics of all relevant reactions related to this system (see also Supporting Information). Details of the thermodynamics of reaction (1) in the gas phase and the main reaction (1) of 2 $Se_6I_2^{2+}$(solv) to $Se_4I_4^{2+}$(solv) + Se_8^{2+}(solv) observed in solution, is given in Table 6. The calculated value of the free energy (= + 3.8 kJ mol^{-1}) of this dissociation in SO_2 solution is in agreement with the experimental findings, closely matching the observed equilibrium constant.[111] The second most important equilibrium in solution is the dissociation of 2 $Se_4I_4^{2+}$(solv) to $Se_6I_2^{2+}$(solv) and 2 SeI_3^{+}(solv) given by equation (2) (Table 6). An approximate experimental value of (ΔG = +2 kJ mol^{-1}) was obtained from a temperature dependence study [21] of $Se_4I_4^{2+}$ in SO_2 solution which, is at variance with the calculated value of –70.6 kJ mol^{-1}. This is due to the fact that the gas phase calculations are not isodesmic, the ionic charges being different in the reactants and products. Thus the calculated gas and solution values for reactions of this type are not reliable by the methods used in this study.

Crystals of $Se_6I_2(AsF_6)_2.2SO_2$(s) were prepared by cooling the equilibrium mixture in liquid SO_2 and slowly warming to room temperature. Mixtures were obtained on attempted crystallisation of solutions of $Se_6I_2(AsF_6)_2$ and all its equilibrium products in liquid SO_2 at room temperature without prior crystal growth at low temperatures. The IR spectrum of $Se_6I_2(AsF_6)_2.2SO_2$ (s) showed that some SO_2 was retained on grinding at room temperature. However prolonged evacuation of $Se_6I_2(AsF_6)_2.2SO_2$(s) resulted in decomposition.[22] These facts are consistent with the thermodynamic estimates given in Table 6, which predict that solid $Se_6I_2(AsF_6)_2.2SO_2$ at low temperatures (i.e.203K) is stable towards dissociation to $Se_4I_4(AsF_6)_2$(s), $Se_8(AsF_6)_2.⅓\ SO_2$(s) and SO_2(l) [ΔG^o(S13)/kJ $mol^{-1} \approx +15$ at 203K; stability

decreasing to ΔG^o(S13)/kJ mol^{-1} ≈ –6 at higher temperature (i.e. 298K)].[112] When the product, SO_2 is in its *gaseous* form [reaction (S42)], stability is much enhanced at low temperatures, being (ΔG^o(S42) /kJ mol^{-1} ≈ +34 at 203K) whilst much reduced (ΔG^o(S42) /kJ mol^{-1} ≈ – 18) at 298 K. Stability of the solvates towards loss of SO_2(l), *without* dissociation, according to equations (3) and (5) (Table 6), is seen with ΔG^o(3)/kJ mol^{-1} predicted to be +17 at 203K and +6 at 298K; ΔG^o(5)/kJ mol^{-1} predicted to be +3 at 203K and +1 at 298K. The data suggest the solvates becomes more unstable at higher temperatures. (Similar trends are found for loss of SO_2(g), as in reactions (4) and (6) with ΔG^o(4)/kJ mol^{-1} predicted to be +28 at 203K, 0 at 298K; ΔG^o(6)/kJ mol^{-1} predicted to be +4 at 203K,+0 at 298K).

It seems that $Se_6I_2(AsF_6)_2.2SO_2$(s) is an example of an isolated and characterized SO_2 solvate for which the corresponding non solvated parent salt $Se_6I_2(AsF_6)_2$(s) is thermodynamically unstable at all temperatures, the latter disproportionating according to equation (S6) in Table 6 (ΔG^o(S6) /kJ mol^{-1} ≈ – 15 at 203K and – 17 at 298K).

It is the second such example for a non aqueous solvate. The first is CuI_2•$4NH_3$ which has an unsolvated parent, CuI_2, which is thermodynamically unstable [113] due to decomposition to CuI and Cu. This situation is also rare for the numerous hydrates [114]

Thermodynamic estimates for dissociation reactions of $Se_6I_2^{2+}$ and $Se_4I_4^{2+}$ in all phases (reactions S18, S22, S26, S30, S34, S38, S47, S51 and S55 are given in the Supporting Information). The possibility of preparing $Se_4I_2(AsF_6)_2$.(s), or an SO_2 solvate is also discussed.

Reaction of $(Se_4)[AsF_6]_2$ and Br_2 in SO_2. The natural–abundance ^{77}Se NMR spectra of solutions with Se_4^{2+}/Br_2 ratio of 1:1.1 at –70C contained peaks attributable to Se_4^{2+} Se_8^{2+}, 1,1,3–$Se_3Br_3^+$,[34] and two peaks at 1596 and 1126 that we assign to 1,1,4,4–$Se_4Br_4^{2+}$ by comparison with those of 1,1,4,4–$Se_4I_4^+$ (see Tables 3 and 7).

The solution from the 1:2.1 sample contained these species, but in addition peaks at 1317, 1205, 1165 and 1082, which we tentatively assign to cyclic Se_7Br^+, as they are similar to the **D** set in the spectrum of the equilibrium mixture due to the dissociation of 1,4–$Se_6I_2^{2+}$ (see Tables 4 and 7). The peaks were broader in the Se_4^{2+}/Br_2 spectra and no satellites due to ^{77}Se–^{77}Se coupling could be detected. Solutions from the 1:2.9 reaction contained only 1,1,3–$Se_3Br_3^+$. Solutions for 1:4.0 and 1:5.0 ratios contained broad peaks attributable to $Se_2Br_5^+$ and $SeBr_3^+$.

The calculated ^{77}Se NMR chemical shifts for 1,1,4,4–$Se_4Br_4^{2+}$ are consistent with the experimental values (see Table 7). The optimized structure of 1,1,4,4–$Se_4Br_4^{2+}$ is similar to that of 1,1,4,4–$Se_4I_4^{2+}$ with a similar Se–Se bond alternation (See Figure 11 and Supporting Information). Given the complexities of calculated chemical shifts for Se_7I^+, we did not carry out a related study for Se_7Br^+.

Conclusions

Upon dissolving $(Se_6I_2)[AsF_6]_2\cdot 2SO_2$ in SO_2(l) in a sonic bath, a solution was formed containing 1,4–$Se_6I_2^{2+}$ in equilibrium with Se_n^{2+} (n = 4, 8, 10) SeI_3^+, 1,1,4,4–$Se_4I_4^{2+}$ and 5 hitherto unknown binary selenium iodine cations. Solid crystalline $(Se_6I_2)[AsF_6]_2\cdot 2SO_2$ was regenerated by cooling the equilibrium mixture from –70 ^{o}C to –80 ^{o}C and allowing it stand at R.T. for one day. This very unusual situation is reminiscent of elemental solid sulfur, which melts to give a complex equilibrium of S_8 with numerous other sulfur species, but upon crystallization regenerates solid S_8.

The composition of the equilibrium mixture was studied by ^{77}Se NMR spectroscopy at –70 ^{o}C using both natural–abundance ^{77}Se samples and those containing selenium enriched in the ^{77}Se–isotope (enrichment 92 %). The use of enriched selenium enabled the first recording

of ^{77}Se-^{77}Se COSY spectrum. The NMR spectra show the presence of 1,4–$Se_6I_2^{2+}$, SeI_3^+, 1,1,4,4–$Se_4I_4^{2+}$, Se_{10}^{2+}, Se_8^{2+}, and Se_4^{2+} for which chemical shifts and coupling patterns are known. However, previous work on 1,4–$Se_6I_2^{2+}$ and 1,1,4,4–$Se_4I_4^{2+}$ was based only on 1D NMR with natural abundance ^{77}Se samples. Their identity in solution is confirmed by the present study. Previous assignments of ^{77}Se chemical shifts of Se_8^{2+} were also based on 1D NMR, and these have been revised in our more complete investigation. The ^{77}Se chemical shifts of the cations were calculated at the relativistic ZORA rPBE level utilizing large QZ4P basis sets, the first such study of halidopolychalcogen species. The theoretical chemical shift predictions and in particular calculations, which include solvent molecules explicitly yield a reasonable agreement with the experimental chemical shifts.

The structure and bonding in 1,4–$Se_6I_2^{2+}$ and 1,1,4,4–$Se_4I_4^{2+}$ were explored by hybrid DFT calculations. The pronounced Se–Se bond alternation and thermodynamically stable 4pπ–4pπ and 5pπ–4pπ Se–Se and Se–I π bonds were shown to be formed by positive charge delocalization via $p^2 \rightarrow \sigma^*$ interactions based on an NBO analysis confirming previously proposed simple qualitative bonding models.[1,22]

In addition to the resonances attributable to previously characterized cations, the ^{77}Se NMR spectra contained 22 other resonances. Their assignments were based on ^{77}Se–^{77}Se COSY, selective irradiation experiments, and spectral simulation that together yield information on the number of the species and their spin systems. By combining this information with the trends in the chemical shifts, with iodine, selenium, and charge balances, as well as with ZORA chemical shift predictions, these resonances were assigned to five hitherto unknown binary selenium–iodine cations. The experimental and DFT data are consistent with the designation of the unknown species as the acyclic 1,1,2–$Se_2I_3^+$, 1,1,6,6–$Se_6I_4^{2+}$, and 1,1,6–$Se_6I_3^+$, as well as cyclic Se_7I^+ and $(4\text{–}Se_7I)_2I^{3+}$.[100] Whereas selenium iodides were once said to be non–existent,[115] now three neutral, one anionic and nine cationic

binary iodides of selenium have been identified. Therefore, there are now as many binary selenium-iodine species as other halogens. However, there are many more examples of the possible $X_mSe_n^{x+}$ (X = halogen) for iodine than for chlorine or bromine (see Table 1), assuming the assignments of the unknowns are correct. There are more new examples for iodine than all other univalent organic derivatives (see Table 8). We note the absence of $I_2Se^+(Se)_nSe^+I_2$ when *n* is odd but the presence of the species, when *n* is even. Bond alternation arising from positive charge delocalization is reinforced for even *n* but cancels for odd *n* (see Scheme 1).[1c] Thus, cations in which positive charge delocalization and consequent bond alternation occur are favored.

Despite of the apparent consistency of the experimental and theoretical results the completely unambiguous assignment of the chemical identities of the unknown cations remains a computational challenge for future study.

In the absence of any experimental thermodynamic data regarding the stability of $Se_6I_2(AsF_6)_2 \cdot 2SO_2$(s) towards loss of SO_2 and its disproportionation to $Se_4I_4(AsF_6)_2$.(s), $Se_8(AsF_6)_2 \cdot 1/3SO_2$.(s) and SO_2 was estimated by Volume–Based Thermodynamics (VBT) and this first application of the Thermodynamic Solvate Difference Rule for non–aqueous solvates. The estimates were consistent with experimental observations, i.e. $Se_6I_2(AsF_6)_2 \cdot 2SO_2$(s) could be handled at room temperature, but stability decreased on increase of temperature and/or prolonged evacuation. $Se_6I_2(AsF_6)_2 \cdot 2SO_2$(s) is the first example of an SO_2 solvate for which the non solvated parent salt, $Se_6I_2(AsF_6)_2$.(s) is not thermodynamically stable disproportionating to $Se_4I_4(AsF_6)_2$.(s) and $Se_8(AsF_6)_2$(s) ($\Delta G^0 \approx -17 \pm 15$ kJ mol^{-1}) . The error ± 15 kJ mol^{-1} here ascribed (and applicable to all the VBT results) renders the corresponding reaction as being absolutely borderline as was observed.

A preliminary solution ^{77}Se natural abundance study of the reaction of $Se_4(AsF_6)_2$ with bromine in various ratios contained resonances attributable to 1,1,4,4–$Se_4Br_4^{2+}$ by comparison

with ^{77}Se chemical shifts, and a general agreement of the calculated and observed ^{77}Se chemical shifts. A second set of resonances was attributable to cyclic Se_7Br^+ by comparison to that of cyclic Se_7I^+ (**D**). These results imply that numerous binary chlorido–, bromido–, and organic univalent group polyselenium cations exist, albeit in solution, and warrant a more extensive and thorough study.

Acknowledgments

The financial support from Academy of Finland, Emil Aaltonen Foundation, Helsingin Sanomain 100–vuotissäätiö, and NSERC is gratefully acknowledged. We also thank the Finnish Centre of Scientific Computing for allocation of computational resources. Professor Jenkins thanks the University of Warwick for facilities kindly provided.

Supporting information available

The coordinates of the optimized cation–solvent clusters, Calculated Absolute Energies, Optimized structure of 1,1,4,4-$Se_4Br_4^{2+}$, Rejected alternative assignment of the resonances in groups A-E, MP2 calculations, SeI_3^+ with 9 SO_2 molecules, Thermodynamics and calculation of reaction energetics, NBO result. A list of binary electrically neutral, cationic, and anionic sulfur- and tellurium – halogen (X = Cl, Br, I) species.

References and notes

(1) (a) Klapötke, T.; Passmore, J. *Acc. Chem. Res.* **1989**, *22*, 234, and references therein. (b) Burford, N.; Passmore, J.; Sanders, J.C.P., in Leibman, J.F.; Greensberg, A., Eds. *From Atoms to Polymers, Isoelectronic Analogies*, VCH: Boca Raton, FL 1989, p. 53, and references therein. (c) Passmore, J. in Steudel, R., Ed. *The Chemistry of Inorganic*

Ring Systems. Studies in Inorganic Chemistry, Elsevier: New York 1992; Vol. 19, p.373, and references therein.

(2) For the reaction:

$$2\text{RSe–I(s)} \xrightarrow{\Delta_R H^o} \text{RSe–SeR(s)} + \text{I–I(s)}$$

when the standard states of RSe–I and RSe–SeR are solids, a thermochemical cycle shows that the enthalpy change $\Delta_R H^o$ is given by:

$$\Delta_R H^o = 2\,\Delta_{sub}H^o(\text{RSeI, s}) + 2\,\text{BDE(Se–I)} - \text{BDE(Se–Se)} - \text{BDE(I–I)} - \Delta_{sub}H^o(\text{RSeSeR, s}) - \Delta_{sub}H^o(\text{I}_2\text{, s})$$

where BDE represents the bond dissociation enthalpy. Alternatively, for the reaction:

$$2\text{RSe–I(l)} \xrightarrow{\Delta_R H^o} \text{RSe–SeR(l)} + \text{I–I(s)}$$

when the standard states of RSe–I and RSe–SeR are liquids, a thermochemical cycle shows that the enthalpy change $\Delta_R H^o$ is given by:

$$\Delta_R H^o = 2\,\Delta_{vap}H^o(\text{RSeI, s}) + 2\,\text{BDE(Se–I)} - \text{BDE(Se–Se)} - \text{BDE(I–I)} - \Delta_{vap}H^o(\text{RSeSeR, s}) - \Delta_{sub}H^o(\text{I}_2\text{,s})$$

Except in the case of very bulky R (destabilising R–Se–Se–R) for which there is no strain in the R–Se–I and in R–Se–Se–R, the gas phase BDE enthapy terms convieniently cancel out (i.e. 2BDE(Se–I) – BDE(Se–Se) – BDE(I–I) ≈ 0 kJ mol^{-1} and the sublimation enthalpy, $\Delta_{sub}H^o(\text{I}_2\text{, s})$ (62.3 kJ mol^{-1}) is, therefore, the major factor in accounting for the instability of RSeI molecules.

(3) (a) Greenwood, N.N.; Straughan, B.P. *J. Chem. Soc. A* **1966**, 962. (b) Passmore, J.; Taylor, P. *J. Chem. Soc., Dalton Trans.* **1976**, 804.

(4) (a) Bowen, H. J. M. *Nature* **1953**, *172*, 171. (b) Lachman, F. *Nature* **1953**, *172*, 499.

(5) (a) Brockway, L. O.; Pauling, L. *Proc. Natl. Acad. Sci.* **1933**, *19*, 68. (b) Braune, H.; Knoke, S. *Z. Physik. Chem.* **1933**, *B21*, 297.

(6) (a) Akishin, P. A.; Spiridonov, V. P.; Mishulina, R. A. *Vestn. Mosk. Univ., Ser. 2 Khim.* **1962**, *17*, 23. (b) Fernholt, L.; Haaland, A.; Seip, R.; Kniep, R.; Korte, L. *Z. Naturforsch.* **1983**, *38B*, 1072.

(7) Kniep, R.; Korte, L.; Mootz, D. *Z. Naturforsch.* **1983**, *B38*, 1.

(8) (a) Born, P.; Kniep, R.; Mootz, D.; Hein, M.; Krebs, B. *Z. Naturforsch.* **1981**, *36B*, 1516. (b) Kniep, R.; Korte, L; Mootz, D. *Z. Naturforsch.* **1981**, *36B*, 1660.

(9) Born, P.; Kniep, R.; Mootz, D. *Z. Anorg. Allg. Chem.* **1979**, *451*, 12.

(10) Gopal, M.; Milne, J. *Inorg. Chem.* **1992**, *31*, 4530.

(11) Edwards, A. J.; Jones, G. R. *Chem. Commun.* **1968**, 346.

(12) (c) Christian, B. H.; Collins, M. J.; Gillespie, R. J.; Sawyer, J. F. *Inorg. Chem.* **1986**, *25*, 777.

(13) (a) Stork-Blaisse, B. A.; Romers, C. *Acta Crystallogr.* **1971**, *B27*, 386. (b) Jones, P. G.; Schelbach, R.; Schwarzmann, E. *Acta Crystallogr.* **1987**, *C43*, 607.

(14) Bakshi, P.; Boyle, P. D.; Cameron, T. S.; Passmore, J.; Schatte, G.; Sutherland, G. *Inorg. Chem.* **1994**, *33*, 3849.

(15) Faggiani, R.; Gillespie, R. J.; Kolis, J.; Malhotra, K. C. *Chem. Commun.* **1987**, 591.

(16) Passmore, J.; Richardson, E. K.; Whidden, T. K.; White, P. S. *Can. J. Chem.* **1980**, *58*, 851.

(17) Passmore, J.; Tajik, M.; White, P. S. *J. Chem. Soc., Chem. Commun.* **1988**, 175.

(18) Murchie, M. P.; Passmore, J.; White, P. S. *Can. J. Chem.* **1987**, *65*, 1584.

(19) Johnson, J. P.; Murchie, M.; Passmore, J.; Tajik, M.; White, P. S.; Wong, C.-M. *Can. J. Chem.* **1987**, *65*, 2744.

(20) (a) Nandana, W. A. S.; Passmore, J.; White, P. S.; Wong, C.-M. *J. Chem. Soc., Chem. Commun.* **1982**, 1098. (b) Nandana, W. A. S.; Passmore, J.; White, P. S.; Wong, C.-M. *Inorg. Chem.* **1990**, *29*, 3529.

(21) Carnell, M. M.; Grein, F.; Murchie, M.; Passmore, J.; Wong, C.-M. *J. Chem. Soc., Chem. Commun.* **1986**, 225.

(22) (a) Passmore, J.; White, P. S.; Wong, C.-M. *J. Chem. Soc., Chem. Commun.* **1985**, 1178. (b) Nandana, W. A. S.; Passmore, J.; White, P. S.; Wong, C.-M. *Inorg. Chem.* **1989**, *28*, 3320. (c) Wong, C-M. Ph.D. Thesis, Univ. of New Brunswick, 1988.

(23) (a) Nandana, W. A. S.; Passmore, J.; White, P. S. *J. Chem. Soc., Chem. Commun.* **1983**, 526. (b) Beck, J.; Marschall, T. *Z. Kristallogr.* **1995**, *210*, 265.

(24) Mahjoub, A. R.; Leopold, D.; Seppelt, K. *Z. Anorg. Allg. Chem.* **1992**, *618*, 83.

(25) Mahjoub, A. R.; Zhang, X.; Seppelt, K. *Chem.− Eur. J.* **1995**, *1*, 261.

(26) Krebs, B.; Luehrs, E.; Willmer, R.; Ahlers, F. P. *Z. Anorg. Allg. Chem.* **1991**, *592*, 17.

(27) Gillespie, R. J.; Kent, J. P.; Sawyer, J. F. *Inorg. Chem.* **1990**, *29*, 1251.

(28) (a) Engel, G. *Z. Kristallogr.* **1935**, *90*, 341. (b) Abriel, W. *Acta Crystallogr.* **1986**, *C42*, 1113.

(29) Boyle, P. D.; Godfrey, S. M.; Pritchard, R. G. *J. Chem. Soc., Dalton Trans.* **1999**, 4245.

(30) Stammler, H. G.; Weiss, J. *Z. Naturforsch.* **1989**, *44B*, 1483.

(31) (a) Krebs, B.; Rieskamp, N.; Schaeffer, A. *Z. Anorg. Allg. Chem.* **1986**, *532*, 118. (b) Privett, A. J.; Craig, S. L.; Jeter, D. Y.; Cordes, A. W.; Oakley, R. T.; Reed, R. W. *Acta Crystallogr.* **1987**, *C43*, 2023.

(32) Ahlers, F. P.; Luehrs, E.; Krebs, B. *Z. Anorg. Allg. Chem.* **1991**, *594*, 7.

(33) Czado, W.; Müller, Ulrich *Z. Anorg. Allg. Chem.* **1996**, *622*, 790.

(34) Krebs, B.; Schaeffer, A.; Pohl, S. *Z. Naturforsch.* **1984**, *39B*, 1633.

(35) (a) Sieg, L. *Z. Anorg. Allg. Chem.* **1932**, *207*, 93. (b) Hoard, J. L.; Dickinson, B. N. *Z. Kristallogr.* **1933**, *84*, 436. (c) Abriel, W. *Z. Naturforsch.* **1987**, *42B*, 415.

(36) Krebs, B.; Luehrs, E.; Ahlers, F. P. *Angew. Chem.* **1989**, *101*, 190.

(37) Boyle, P. D.; Cross, W. I.; Godfrey, S. M.; McAuliffe, C. A.; Pritchard, R. G.; Teat, S. J. *J. Chem. Soc., Dalton Trans.* **1999**, 2845.

(38) Hasche, S.; Reich, O.; Beckmann, I.; Krebs, B. *Z. Anorg. Allg. Chem.* **1997**, *623*, 724.

(39) Hauge, S.; Maroey, K. *Acta Chem. Scand.* **1996**, *50*, 399.

(40) Krebs, B.; Ahlers, F. P.; Luehrs, E. *Z. Anorg. Allg. Chem.* **1991**, *597*, 115.

(41) Hauge, S.; Janickis, V.; Maroy, K. *Acta Chem. Scand.* **1998**, *52*, 1104.

(42) Hauge, S.; Maroy, K.; Oedegaard, T. *Acta Chem. Scand.* **1988**, *A42*, 51.

(43) Janickis, V.; Törnroos, K. W.; Herberhold, M.; Songstad, J.; Milius, W. *Z. Anorg. Allg. Chem.* **2002**, *628*, 1967.

(44) Brownridge, S.; Krossing, I.; Passmore, J.; Jenkins, H. D. B.; Roobottom, H.K. *Coord. Chem. Rev.* **2000**, *197*, 397.

(45) Cameron, T.S.; Deeth, R.J.; Dionne, I.; Du, H.; Jenkins, H.D.B.; Krossing, I.; Passmore, J.; Roobottom, H.K. *Inorg. Chem.* **2000**, *39*, 5614.

(46) Brooks, W.V.F.; Cameron, T.S.; Parsons, S.; Passmore, J.; Schriver, M.J. *Inorg. Chem.* **1994**, *33*, 6 230.

(47) Krossing, I.; Passmore, J. *Inorg. Chem.* **2004**, *43*, 1000.

(48) (a) Brownridge, S.; Calhoun, L.; Laitinen, R.S.; Passmore, J.; Pietikäinen, J.; Saunders, J. *Phosphorus Sulfur Silicon Relat. Elem.* **2001**, *168/169*, 105. (b) Laitinen; R.S.; Brownridge; S.; Calhoun; L.; Passmore; J.; Pietikäinen; J.; Rautiainen; J.M.; Suontamo; R.J.; Saunders; J.; Schrobilgen; G.J.; Tuononen; H.; Valkonen; J. U., International Conference on Heteroatom Chemistry, Riverside, USA, August 12-16, 2007. *Abstracts*, Oral 3.

(49) (a) Schreckenbach, G.; Ruiz-Morales,Y.; Ziegler, T. *J. Chem. Phys.* **1996**, *104*, 8605. (b) Nakanishi, W.; Hayashi,S. *J. Phys. Chem. A* **1999**, *103*, 6074. (c) Wilson, P. *J. Mol. Phys.* **2001**, *99*, 363. (d) Bayse, C. A. *Inorg. Chem.* **2004**, *43*, 1208. (e) Chesnut,

D. B. *Chem. Phys.* **2004**, *305*, 237. (f) Maaninen, T.; Tuononen, H. M.; Kosunen, K.; Oilunkaniemi, R.; Hiitola, J.; Laitinen, R. S.; Chivers, T. *Z. Anorg. Allg. Chem.* **2004**, *630*, 1947. (g) Poleschner, H.; Seppelt, K. *Chem. Eur. J.* **2004**, *10*, 6565. (h) Bayse, C. A. *J. Chem. Theory Comput.* **2005**, *1*, 1119. (i) Bhabak, K. P.; Mugesh, G. *Chem. Eur. J.* **2007**, *13*, 4594.

(50) Demko, B. A.; Eichele, K.; Wasylishen, R. E. *J. Phys. Chem. A* **2006**, *110*, 13537.

(51) Rautiainen, J. M.; Way, T. C.; Schatte, G.; Passmore, J.; Laitinen, R. S.; Suontamo, R. J.; Valkonen, J. *Inorg. Chem.* **2004**, *44*, 1904.

(52) Tattershall, B. W.; Sandham, E. L. *J. Chem. Soc., Dalton Trans.* **2001**, 1834.

(53) Murchie, M. P. Ph.D. Thesis, Univ. of New Brunswick, 1986.

(54) Brownridge, S.; Crawford, M.-J..; Du, H.; Harcourt, R. D.; Knapp, C.; Laitinen, R. S.; Passmore, J.; Rautiainen, J. M.; Suontamo, R. J.; Valkonen, J. *Inorg. Chem.* **2007**, *46*, 681.

(55) Krossing, I.; Passmore, J. *Inorg.Chem.* **1999**, *38*, 5203.

(56) (a) Jenkins, H. D. B.; Roobottom, H. K.; Passmore, J.; Glasser, L. *Inorg. Chem.* **1999**, *38*, 3609. (b) Jenkins, H. D. B.; Tudela, D.; Glasser, L. *Inorg. Chem.* **2002**, *41*, 2364. (c) Jenkins, H. D. B.; Glasser, L. *Inorg. Chem.* **2003**, *42*, 8702. (d) Glasser, L; Jenkins, H. D. B, *Thermochim. Acta*, **2004**, *414*, 125 . (e) Jenkins, H. D. B. *J. Chem. Edu*., **2005**, *82*, 950. (f) Jenkins, H. D. B.; Glasser, L.; Klapötke, T. M.; Crawford, M-J.; Bhasin, K.; K.; Lee, J; Schrobilgen, G. J.; Sunderlin, L.; Liebman, J. F. *Inorg. Chem.* **2004**, *43*, 6238. (g) Jenkins, H. D. B.; Liebman, J. F. *Inorg. Chem.* **2005**, *44*, 6359. (h) Glasser, L; Jenkins, H. D. B. *Chem. Soc. Rev.*, **2005**, *34*, 866.

(57) (a) Decken, A.; Jenkins, H. D. B.; Nikiforov, G. B. ; Passmore, J. P., *Dalton Trans*, **2004**, 2496. (b) Decken, A.; Ilyin, E. G.; Jenkins, H. D. B.; Nikiforov, G. B. ; Passmore, J. P., *Dalton Trans*, **2005**, 3039. (c) Decken, A.; Jenkins, H. D. B.; Knapp,

C.; Nikiforov, G. B. ; Passmore, J. P.; Rautiainen, J. Mikko. *Angewandte Chemie, Int. Ed.,* **2005**, *117,* 8172. (d) Bhasin, K.; K.; Crawford, M-J.; Jenkins, H. D. B.; Klapötke, T. M.; Liebman, J. F. *Z. Anorg. Allg. Chem.* **2006**, *632*, 897.(e) Decken, A; Jenkins, H. D. B.; Mailman, A.; Passmore, J.; Shuvaev, K. V. *Inorg. Chim. Acta*, **2008**, *361*, 521.

(58) (a) Jenkins, H. D. B.; Glasser, L. *J. Am. Chem. Soc*., **2004**, *126*, 15809. (b) Jenkins, H. D. B.; Glasser, L. *Inorg. Chem*., **2002**, *41*, 4378. (c) Glasser, L.; Jenkins, H. D. B., *Inorg. Chem*., **2007**, *46*, 9768. (d) Jenkins, H. D. B.; Liebman, J. F. *J. Chem. Eng. Data.,* **2008**, in proof. (Invited contribution to R. H. Stokes Festschrift Edition).

(59) (a) Passmore, J.; Richardson, E.K.; Taylor, R. *J. Chem. Soc., Dalton Trans.* **1976**, 1006. (b) Murchie, M.P.; Passmore, J. *Inorg. Synth.* **1986**, *24*, 76. (c) Murchie, M. P.; Kapoor, R.; Passmore, J.P.; Schatty, G.; Way, T. *J. Inorg. Synth*. 1997, *3*, 102.

(60) The temperature of the sonic bath needs to be carefully controlled, because higher temperatures may lead to dangerously high pressures inside the NMR tube.

(61) Murchie, M. P.; Sutherland, G. W.; Kapoor, R.; Passmore, J. *J. Chem. Soc. Dalton Trans.***1992**, 3, 503.

(62) Burns, R. C.; Gillespie, R. J. *Inorg. Chem.* **1982,** 21, 3877.

(63) In the course of this study spanning more than 10 years both 1D and 2D NMR spectra have been recorded on a variety of instruments: VARIAN UNITY 200 (University of New Brunswick, Bruker AM250 and AM500 (McMaster University), as well as Bruker DSX300 and DXP400 (University of Oulu). All spectroscopic information is consistent with the actual spectra reported in this contribution.

(64) The intensity measurements were repeated by using the pulse width of 4.0 μs (nuclear tip angle of 23°) but keeping acquisition time and the relaxation delay constant. There were virtually no changes in the intensities.

(65) PERCH, Version 2/07, Perch Solutions, Ltd., Kuopio, Finland, 2007.

(66) Santry, D. P.; Mercier, H. P. A.; Schrobilgen, G. J. *ISOTOPOMER, A Multi-NMR Simulation Program,* V*ersion 3.02NTF*.; Snowbird Software, Inc.: Hamilton, ON, 2000.

(67) (a) Ahlrichs, R.; Bär, M.; Häser, M.; Horn, H.; Kölmel, C. *Chem. Phys. Lett.* **1989**, *162*, 165. (b) Aldrichs, R. et al. TURBOMOLE, *Program Package for ab initio Electronic Structure Calculations*, version 5.9; http://www.cosmologic.de, Germany, 2006.

(68) (a) Perdew, J. P.; Burke, K.; Ernzerhof, M. *Phys. Rev. Lett.* **1996**, *77*, 3865; **1997**, *78*, 1396 (E). (b) Perdew, J. P.; Ernzerhof, M.; Burke, K. *J. Chem. Phys*. **1996**, *105*, 9982. (c) Adamo, C.; Barone, V. *J. Chem. Phys.* **1999**, *110*, 6158.

(69) (a) Dunning, T. H., Jr. *J. Chem. Phys.* **1989**, *90*, 1007. (b) Woon, D. E.; Dunning, T. H., Jr. *J. Chem. Phys.* **1993**, *98*, 1358. (c) Wilson, A.K.; Woon, D. E.; Peterson, K. A.; Dunning, T. H., Jr. *J. Chem. Phys.* **1999**, *110*, 7667.

(70) (a) Martin, J. M. L.; Sundermann, A. *J. Chem. Phys.* **2001**, *114*, 3408. (b) Bergner, A.; Dolg, M.; Kuechle, W.; Stoll, H.; Preuss, H. *Mol. Phys.* **1993**, *80*, 1431.

(71) Amos, R. D.; Bernhardsson, A.; Berning, A.; Celani, P.; Cooper, D. L.; Deegan, M. J. O.; Dobbyn, A. J.; Eckert, F.; Hampel, C.; Hetzer, G.; Knowles, P. J.; Korona, T.; Lindh, R.; Lloyd, A. W.; McNicholas, S. J.; Manby, F. R.; Meyer, W.; Mura, M. E.; Nicklaß, A.; Palmieri, P.; Pitzer, R.; Rauhut, G.; Schütz, M.; Schumann, U.; Stoll, H.; Stone, A. J.; Tarroni, R.; Thorsteinsson, T.; Werner, H.-J. MOLPRO, Revision 2002.6.

(72) (a) Klamt, A.; Jones, V. *J. Chem. Phys.* **1996**, *105*, 9972. (b) Klamt, A. *J. Phys. Chem.* **1995**, *99*, 2224. (c) Klamt, A.; Schüürmann, G. *J. Chem. Soc., Perkin Trans.* **1993**, *2*, 799.

(73) (a) Lide, D. R., Ed. *CRC Handbook of Chemistry and Physics*, 83rd ed., CRC Press: Boca Raton, FL 2002, p. 6-154. (b) Lide, D. R., Ed. *CRC Handbook of Chemistry and Physics*, 74th ed., CRC Press: Boca Raton, FL 1993, p. 6-106.

(74) Glendening, E. D.; Badenhoop, J. K.; Reed, A. E.; Carpenter, J. E.; Bohmann, C. M.; Morales, C. M.; Weinhold, F. *NBO*, Version 5.0; Theoretical Chemistry Institute, University of Wisconsin, Madison, WI, 2001.

(75) R. W. F. Bader et. al. AIMPAC: A Suite of programs for the AIM theory, McMaster University, Hamilton, Ontario, Canada L8S 4M1, http://www.chemistry.mcmaster.ca/aimpac.

(76) Wolff, S. K.; Ziegler, T.; van Lenthe, E.; Baerends, E. J. *J. Chem. Phys.* **1999**, *110*, 7689.

(77) (a) te Velde, G.; Bickelhaupt, F. M.; van Gisbergen, S. J. A.; Fonseca Guerra, C.; Baerends, E. J.; Snijders, J. G.; Ziegler, T. *J. Comput. Chem.* **2001**, *22*, 931. (b) Fonseca Guerra, C.; Snijders, J. G.; te Velde, G.; Baerends, E. *J. Theor. Chem. Acc.* **1998**, *99*, 391. (c) ADF2005.01b, SCM, Theoretical Chemistry, Vrije Universiteit, Amsterdam, The Netherlands, http://www.scm.com.

(78) Hammer, B.; Hansen, L. B.; Norskov, J. K. *Phys. Rev.* **1999**, *B59*, 7413.

(79) Schreckenbach, G.; Ziegler, T. *Int. J. Quantum Chem.* **1996**, *60*, 753.

(80) Eichkorn, K.; Weigend, F.; Treutler, O.; Ahlrichs, R. *Theor. Chem. Acc.* **1997**, *97*, 119.

(81) Weigend, F.; Ahlrichs, R. *Phys. Chem. Chem. Phys.* **2005**, *7*, 3297.

(82) (a) Schrobilgen, G.J.; Burns, R.C.; Granger, P. *J. Chem. Soc., Chem. Commun.*, **1978,** 957. (b) Collins, M.J.; Gillespie, R.J.; Sawyer, J.F.; Schrobilgen, G.J. *Inorg. Chem.* **1988**, *25*, 2053.

(83) Burns, R. C.; Collins, M. J.; Gillespie, R. J.; Schrobilgen, G. J. *Inorg. Chem.* **1986**, *23*, 4465.

(84) 1,4-$Se_6I_2^{2+}$: 1313 and 484 ppm (intensity ratio 2:1); 1,1,4,4-$Se_4I_4^{2+}$: 1554 and 979 ppm (1:1); SeI_3^+: 836 ppm.[21] Se_4^{2+}: 1936 ppm.[82] Se_8^{2+}: 1971, 1522, 1197,1071, and 1046 ppm (intensity ratio 2:2:1:2:1).[83]

(85) Tuononen, H. M.; Suontamo, R.; Valkonen, J.; Laitinen, R. S. *J Phys. Chem. A* **2004**, *108*, 5670.

(86) Relative AIM bond orders have been determined from calculated electron densities at bond critical points by calibrating the results with respect to species with well defined bond orders. Se-Se bonds were calibrated against bonds in $(Se_3Br_3)^+$ and Se_2Me_2 and Se-I bonds against bonds in $(I_2Se\text{-}I\text{-}SeI_2)^+$, Me_3CSeI, and SeI_2^+ according to the procedure given in Ref. 54.

(87) (a) Autschbach, J.; Le Guennic, B. *Chem.–Eur. J.* **2004**, *10*, 2581. (b) Kaupp, M.; Bühl, M.; Malkin, V. G., Eds. *Calculation of NMR and EPR Parameters, Theory and Applications*, Wiley-VCH: Weinheim, 2004.

(88) Bagno, A.; Casella, G.; Saielli, G. *J. Chem. Theory Comput.* **2006**, *2*, 37.

(89) The geometry optimizations reveal that many cations show several conformations that are lying relatively close in energy. They are denoted by a set of numerals $\boldsymbol{n_m}$ (***n*** indicates the identification number of the cation, as defined in the main text and the subscript ***m*** identifies their different conformations, as shown in Figure 8.

(90) Belin, C. H. E.; Charbonnel, M. M. *Inorg. Chem.* **1982**, *21*, 2504.

(91) The free energies of conformations in the gas phase have been calculated as G_{gas} = E[CCSD(T)] + $G_{corr.}^{203K}$ (PBE0) and free energies in solution as G_{SO2} = G_{gas} + $G_{solv.}$(PBE0/COSMO).

(92) Koch, W.; Holthausen, M. C. *A Chemist's Guide to Density Functional Theory*, 2nd ed.; Wiley-VHC: Weinheim, 2001.

(93) (a) Passmore, J.; Taylor, P.; Whidden, T. K.; White, P. S. *Chem. Commun.* **1976**, 689. (b) Passmore, J.; Sutherland, G.; Taylor, P.; Whidden, T. K.; White, P. S. *Inorg. Chem.* **1981**, *20*, 3839.

(94) (a)Passmore, J.; Sutherland, G.; White, P. S. *J. Chem. Soc., Chem. Commun.* **1979**, 901. (b) Passmore, J.; Sutherland, G.; White, P.S., *Inorg. Chem.* **1982**, *21*, 2717.

(95) A partially optimized 1,1,4,4-$Se_4I_4^{2+}$ structure where Se2···I contacts of the other iodine atom at both ends of the chain structure are constrained to the experimental Se2···I distance of 1,4-$Se_6I_2^{2+}$ so that 1,1,4,4-$Se_4I_4^{2+}$ forms a cluster-like structure was calculated to be less stable than the optimized structure by 6.5 kJ/mol at CCSD(T)/(SDB)-cc-pVTZ level. This indicates that 1,1,4,4-$Se_4I_4^{2+}$ does not readily adopt a cluster-like structure on its own in the absence of environmental effect (e.g. solvent or crystal lattice).

(96) Collins, M. J.; Gillespie, R. J.; Sawyer, J. F. *Acta Crystallogr.* **1988**, *C44*, 405.

(97) Burns, R. C.; Chan, W.-L.; Gillespie, R. J.; Luk, W.-C.; Sawyer, J. F.; Slim, D. R. *Inorg. Chem.* **1980**, *19*, 1432.

(98) The bond alternation can be rationalized in terms of the relative positive charge carried by the selenium atoms in question. In 1,1,4,4-$Se_4I_4^{2+}$ the four selenium atoms carry the charge of +0.86 (on the average, +0.22/Se atom). In 1,4-$Se_6I_2^{2+}$ the total charge of the six selenium atoms is +1.38 (on the average +0.23/Se atom). Therefore, the bond alternations in both cations are similar. Se_{10}^{2+} shows a bicyclic structure. In the six-atomic ring fragment, the total charge +1.38 (average +0.23/Se atom) and thus the bond alternation is very similar to that observed in both $Se_4I_4^{2+}$ and $Se_6I_2^{2+}$. By contrast, the four-atomic fragment in Se_{10}^{2+} carries only the charge of +0.62.

Therefore, there is less charge delocalization and the fragment shows a smaller bond alternation.

(99) The ZORA rPBE / QZ4P NMR chemical shifts (vacuum/explicit solvent; ppm) for the low-lying conformations of selenium-iodine cations: The three conformations of 1,1,6,6-$Se_6I_4^{2+}$ [for the numbering of atoms, see Figure 18(b)]: Conformation **8$_1$**: Se1 1205/995, Se2 1135/1080, Se3 1537/1423, Se4 1542/1533, Se5 1116/1105, Se6 1128/1044. Conformation **8$_2$**: Se1,Se2 1217/1129, Se3,Se4 1615/1541, Se5,Se6 1128/1084. Conformation **8$_3$:** Se1,Se2 1415/995, Se3,Se4 1825/1373, Se5,Se6 1372/1144. The two conformations of 1,1,6-$Se_6I_3^+$ [for the numbering of atoms, see Figure 18(c)]: Conformation **9$_1$**: Se1 1165/1045, Se2 1734/1638, Se3 1172/1064, Se4 1149/1044, Se5 1304/1162, Se6 1013/889. Conformation **9$_2$**: Se1 1089/1057, Se2 1539/1451, Se3 1190/1114, Se4 1199/1099, Se5 1291/1145, Se6 1035/876. The four conformations of Se_7I^+ (for the numbering of conformations and atoms, see Figure 19): Conformation **10$_1$**: Se1 1719/1646, Se2 1551/1450, Se3 1465/1299, Se4 1562/1433, Se5 957/961, Se6 1247/1176, Se7 1237/1265. Conformation **10$_2$**: Se1 1204/1416, Se2 1391/1326, Se3 1749/1782, Se4 1626/1143, Se5 1185/1158, Se6 1303/1229, Se7 1210/1097. Conformation **10$_3$**: Se1 1170/1208, Se2 1148/1142, Se3 1137/1172, Se4 1080/1016, Se5 1060/1031, Se6 1035/964, Se7 1365/1363. Conformation **10$_4$**: Se1 1061/1120, Se2 1427/1399, Se3 906/986, Se4 1400/1394, Se5 1022/999, Se6 982/1050, Se7 1063/1111.

(100) Several alternatives for the assignment of the resonance groups **A**-**E** to different cations were considered: Group **A**: Se_2I^+; Group **B**: 1,2-$Se_6I_2^{2+}$; Group **C**: 1,1,6,6-$Se_6I_4^{2+}$ (asymmetric rotamer); Group **D**: 1,4-$Se_7I_2^{2+}$, 1,1,7,7-$Se_7I_4^{2+}$ (symmetric rotamer), and Se_7^{2+}; Group **E**: Se_7I^+, 1,1,7,7-$Se_7I_4^{2+}$ (asymmetric rotamer). These assignments were rejected because of a poor fit between the calculated and observed

chemical shifts, inconsistency with coupling information, or chemical implausibility (See Supporting Information for details).

(101) Du Mont, W.-W.; Kubiniok, S.; Peters, K.; Von Schnering, H.G. *Angew. Chem.* **1987,** *99*, 820; *Angew. Chem., Int. Ed. Engl.* **1987**, *26*, 780.

(102) The relative AIM method failed for some reason to give reasonable bond order estimates for 1,1,2-$Se_2I_3^+$ and bond orders calculated from Mayer bond indices have been used instead.[54]

(103) Due to the dynamic nature of the solution environment, it would be desirable to calculate chemical shifts as statistical averages of calculations performed on a representative set of structures obtained from large scale molecular dynamics simulations.[87b]

(104) The calculated chemical shifts of the asymmetric 1,1,6,6-$Se_6I_4^{2+}$ (**8**$_1$) structure that was proposed in our preliminary account [48] to be responsible for the group **C** resonances did not agree well with the observed resonances (see Table 4 and Ref. 99).

(105) Carlowitz, M. V.; Oberhammer, H.; Willner, H.; Boggs, J. E. *J. Mol. Struct.* **1983**, *100*, 161.

(106) Laitinen, R.S.; Pekonen, P.; Suontamo, R.J. *Coord. Chem. Rev.* **1994**, *130*, 1.

(107) Because the enrichment of the ^{77}Se isotope is 92 %, the molar amounts of selenium, iodine, and charge need to be corrected by a factor of 0.92, since only 92 mol of initial $Se_6I_2^{2+}$ is visible in the ^{77}Se NMR spectrum of the final equilibrium mixture

(108) It can be estimated from the recorded intensities that the uncertainty in the molar amounts is *ca*. 5 %.

(109) The values given in parentheses represent the estimated standard deviations in the molar amounts.

(110) (a) Steudel, R.; Mäusle, H.-J. *Angew. Chem.* **1977**, *89*, 114. (b) Steudel, R.; Mäusle, H.-J. *Angew. Chem. Int. Ed. Engl.* **1979**, *18*, 152. (c) Steudel, R. *Z. Anorg. Allg. Chem.* **1981**, *478*, 139. (d) Steudel, R.; Mäusle, H.-J. *Z. Anorg. Allg. Chem.* **1981**, *478*, 156. (e) Mäusle, H.-J.; Steudel, R. *Z. Anorg. Allg. Chem.* **1981**, *478*, 177. (f) Steudel, R.; Passlack-Stephan, S.; Holdt, G. *Z. Anorg. Allg. Chem.* **1984**, *517*, 7. (g) Steudel, R.; Strauss, R.; Koch, L. *Angew. Chem.* **1985**, *97*, 58.

(111) The CCSD(T)/cc-pVTZ//PBE0/cc-pVTZ calculations showed that at 203 K in SO_2 solution, the Gibbs energy of the reaction presented in Eq. 1 is +3.6 kJ mol^{-1}. This corresponds to the equilibrium constant of 0.119 mol dm^{-3}. The calculated equilibrium composition according to Eq. 1 is thus 36 mol-% of 1,4-$Se_6I_2^{2+}$, 32 mol-% of Se_8^{2+}, and 32 mol-% of 1,1,4,4-$Se_4I_4^{2+}$. This approximate result is consistent with the composition of the equilibrium mixture inferred by ^{77}Se NMR spectroscopy taking into consideration the numerous other species that take part in the equilibrium.

(112) The equations and reactions numbered with the prefix 'S' refer to those given in Supporting Information.

(113) Huheey, J. E.; Keiter, E. A.; Keiter, R. L. "Inorganic Chemistry: Principles of Structure & Reactivity", 4th Ed., Harper–Collins, New York, 1993, p.304.

(114) In the vast majority of cases thermodynamically stable hydrates have stable (unsolvated) parent salts. Two exceptions to this rule, frequently quoted [114] are $FeSiF_6$•$6H_2O$ and Na_4XeO_6•$8H_2O$. The hexa– and octa– hydrates whilst themselves being thermodynamically stable do not have stable unsolvated counterparts.

(115) Dasent, W. E. *Non-Existent Compounds;* Marcel Dekker: New York, 1965**,** p. 162.

(116) Poleschner, H.; Seppelt, K. *Angew. Chem. Int. Ed. Engl.* **2008**, *47*, 6461.

(117) Müller, B.; Poleschner, H.; Seppelt, K. *Dalton Trans.* **2008**, 4424.

(118) Laitinen, R.; Steudel, R.; Weiss, R. *J. Chem. Soc., Dalton Trans.* **1986**, 1095. (b)

(119) Faggiani, R.; Gillespie, R. J.; Kolis, J. W. *J. Chem. Soc., Chem. Commun.* **1987**, 592.

Table 1. Binary electrically neutral, cationic, and anionic selenium – halogen (X = Cl, Br, I) species known prior to this work.

Species	Method	Phase [a]	Ref.	Species	Method	Phase [a]	Ref.	Species	Method	Phase [a]	Ref.
(1) Neutral molecules											
SeF_4	ED	g	4	Se_4Cl_{16}	XRD	c	8	SeI_2	NMR	sol	10
SeF_6	ED	g	5	$SeBr_2$	ED	g	6b	ISeSeI	NMR	sol	10
$SeCl_2$	ED	g	6	BrSeSeBr	XRD	c	7	ISeSeSeI	NMR	sol	10
ClSeSeCl	XRD	c	7	Se_4Br_{16}	XRD	c	9				
(2) Cations											
SeF_3^+	XRD	c	11	$SeBr_3^+$	XRD	c	16	$Se_2I_4^{2+}$	XRD	c	20
$SeCl_3^+$	XRD	c	12,13	$Br_2Se^+SeSeBr$	XRD	c	17	$Se_4I_4^{2+}$	NMR	sol	21
$Cl_2Se^+SeSeCl$	XRD	c	14	$Br_2SeBrSeBr_2^+$	XRD	c	18	$Se_6I_2^{2+}$	XRD	c	22
$Se_7SeSeCl^+$	XRD	c	15	SeI_3^+	XRD	c	19	$[Se_6I^+]_n$	XRD	c	22b,23
(3) Anions											
SeF_5^-	XRD	c	24	$Se_4Cl_6^{2-}$	XRD	c	33	$Se_3Br_{10}^{2-}$	XRD	c	36
SeF_6^{2-}	XRD	c	25	$SeBr_4^{2-}$	XRD	c	34	$Se_3Br_{13}^-$	XRD	c	32
$SeCl_4^{2-}$	XRD	c	26	$SeBr_6^{2-}$	XRD	c	35	$Se_4Br_6^{2-}$	XRD	c	33,41
$SeCl_5^-$	XRD	c	27	$Se_2Br_6^{2-}$	XRD	c	34	$Se_4Br_{12}^{2-}$	XRD	c	36
$SeCl_6^{2-}$	XRD	c	28	$Se_2Br_8^{2-}$	XRD	c	36	$Se_4Br_{14}^{2-}$	XRD	c	40,42
$Se_2Cl_4^{2-}$	XRD	c	29	$Se_2Br_9^-$	XRD	c	37	$Se_5Br_{10}^{2-}$	XRD	c	41
$Se_2Cl_6^{2-}$	XRD	c	30	$Se_2Br_{10}^{2-}$	XRD	c	38	$Se_5Br_{12}^{2-}$	XRD	c	40
$Se_2Cl_9^-$	XRD	c	31a	$[Se_2Br_{12}^{2-}]_n$	XRD	c	39	$Se_{16}Br_{18}^{2-}$	XRD	c	43
$Se_2Cl_{10}^{2-}$	XRD	c	30,31	$Se_3Br_8^{2-}$	XRD	c	40	SeI_6^{2-}	IR/R	c	3a
$Se_3Cl_{13}^-$	XRD	c	32								

[a] g = gaseous phase, c = crystalline phase, sol = solution

Table 2. Reaction of $(Se_4)[AsF_6]_2$ and Br_2 in Liquid SO_2.

Tube	$(Se_4)[AsF_6]_2$		Br_2		SO_2	Mole Ratio	
#	g	mmol	g	mmol	g	Se_4^{2+} : Br_2	Precipitate
1	0.75	1.03	0.19	1.19	3.86	1 : 1.1	Unreacted $(Se_4)[AsF_6]_2$ [a]
2	0.78	1.12	0.38	2.36	4.45	1 : 2.1	[b]
3	0.52	0.75	0.35	2.20	3.52	1 : 2.9	[b]
4	0.72	1.04	0.67	4.21	4.26	1 : 4.0	[b]
5	0.73	1.06	0.84	5.27	3.78	1 : 5.0	Dark purple $(Se_2Br_5)[AsF_6]$

[a] $(Se_4)[AsF_6]_2$ was identified by Raman spectroscopy by comparison of the peaks with those reported in the literature.[62]
[b] A precipitate was not observed at room temperature.

Table 3. The ^{77}Se NMR spectroscopic information of 1,4-$Se_6I_2^{2+}$, 1,1,4,4-$Se_4I_4^{2+}$, SeI_3^+, Se_8^{2+}, and Se_4^{2+}.

Species	Experimental chemical shifts (δ, ppm) and coupling constants (*J*, Hz)								ZORA rPBE / QZ4P chemical shifts (ppm)	
	Reson. no [a]	δ	Selenium atom no [b]	No of equiv nuclei	$^1J_{SeSe}$	$^2J_{SeSe}$	$^3J_{SeSe}$	$^4J_{SeSe}$	Vacuum δ[g]	Explicit solvent δ [c,]
$Se_6I_2^{2+}$	12	1313	Se2	4	272, 531	112			1407	1319
	32	476	Se1	2	272	112	7		416	498
$Se_4I_4^{2+}$	6	1548	Se2	2	240, 482	54			1596	1451
	28	978	Se1	2	240	54	16		1163	1008
Se_8^{2+} [d]	1	1970	Se3	2	152.7, 247.6	42.2, 22.6	29.4, 86.8	78.9	2165	2028
	7	1521	Se2	2	64.2, 152.7	91.3, 28.1	29.4, 18.4	46.8	1688	1630
	16	1196	Se1	1	64.2	42.2			1408	1330
	22	1071	Se4	2	15.5, 247.6	28.1, 25.6	86.8	46.8	1156	1127
	24	1046	Se5	1	15.5	22.6	18.4		1193	1175
SeI_3^+	31	830		1					1294	1006
Se_4^{2+}	2	1922 [e]		4					1925 [f]	1955

[a] For numbering of the resonances, see Figure 3. [b] For numbering of atoms in the cations, see Figure 8(a) ($Se_6I_2^{2+}$), Figure 11 ($Se_4I_4^{2+}$), and Figure 12(a) (Se_8^{2+}). [c] Number of explicit solvent molecules: $Se_6I_2^{2+}$ 2; $Se_4I_4^{2+}$ 2; Se_8^{2+} 3; SeI_3^+ 3; Se_4^{2+} 4. [d] The coupling constants for Se_8^{2+} are reported in Ref. 83. See this reference also for the discussion of the relative signs of the constants. [e] Ref. 82. [f] Ref. 85.

Table 4. The assignment of the unknown resonances in the ^{77}Se NMR spectrum of the $Se_6I_2^{2+}$ equilibrium in SO_2.

Reson. Group	Atom no. [a]	Reson. no. [b]	δ (ppm)	$I_{rel.}$	No of equiv nuclei	$^1J_{SeSe}$ (Hz)	$^2J_{SeSe}$ (Hz)	$^3J_{SeSe}$ (Hz)	$^4J_{SeSe}$ (Hz)	Assign.	Vacuum δ	Explicit solvent δ [c]
A	2	8	1486	1	1	176				$Se_2I_3^+$	1456	1342
	1	14	1219	1	1	176					1005	973
B	3,4	17	1181	1	2	142, 259	64	2		$Se_6I_4^{2+}$	1660 [d]	1464 [d]
	1,2	20	1096	1	2	259	106		13		1267 [d]	1054 [d]
	5,6	21	1094	1	2	171, 142	64, 106	118			1207 [d]	1101 [d]
C	2	5	1597	1	1	255, 504	26	18	34	$Se_6I_3^+$	1637 [e]	1545 [e]
	4	11a	1351	1	1	41, 165	26, 52	82			1174 [e]	1072 [e]
	3	11b	1350	1	1	41, 504	21, 97	42			1181 [e]	1089 [e]
	5	18	1170	1	1	165, 214	21	18			1298 [e]	1154 [e]
	1	26	1007	1	1	255	97	82			1127 [e]	1051 [e]
	6	30	873	1	1	214	52	42	34		1024 [e]	883 [e]
D	4,5	19	1149	2	2	20, 109	11, 109	1, 12		Se_7I^+	1237 [f]	1142 [f]
	2,7	23	1064	2	2	83, 85	10, 11	11, 12			1299 [f]	1269 [f]
	1	25	1044	1	1	83	85	1			1289 [f]	1348 [f]
	3,6	27	998	2	2	85, 109	85, 109	1, 11			1228 [f]	1207 [f]
E	2	3	1791	1	1	484, 214	20	33		$(Se_7I)_2I^{3+}$	1525	n.a.
	3	4	1637	1	1	199, 484	3, 23				1473	n.a.
	5	9	1419	1	1	69, 104	3, 173	27, 33			1500	n.a.
	4	10	1374	1	1	104, 199	20	1			1364	n.a.
	1	13	1308	1	1	1, 214	23	1, 27			1377	n.a.
	6	15	1200	1	1	66, 69					1013	n.a.
	7	29	956	1	1	1, 66	173				1005	n.a.

[a] For the numbering of atoms in the cations, see Figure 18 ($Se_2I_3^+$, $Se_6I_4^{2+}$, and $Se_6I_3^+$), Figure 19 (Se_7I^+), and Figure 20 [$(Se_7I)_2I^+$]. [b] For the numbering of the resonances in the ^{77}Se NMR spectrum, see Figure 3. [c] Number of explicit solvent molecules: $Se_2I_3^+$ 3; $Se_6I_4^{2+}$ 6; $Se_6I_3^+$ 3; Se_7I^+ 3. Calculated chemical shift are averaged over [d] three / [e] two / [f] four low energy conformations. See Ref. 99 for chemical shifts of individual conformations.

Table 5. The selenium, iodine, and charge balance of the dissociation products of $Se_6I_2^{2+}$.

		I_{rel} [a]	Abundance	Se mol [b]	I mol [b]	Q mol [b]
$Se_6I_2^{2+}$	1313	313	15	98	33	33
	476	161				
$Se_4I_4^{2+}$	1548	88	8	35	35	18
	978	79				
SeI_3^+	830	61	11	12	36	12
Se_4^{2+}	1925	40	8	35	0	18
Se_8^{2+}	1966	230	20	174	0	44
	1523	221				
	1195	103				
	1071	209				
	1045	103				
Se_{10}^{2+}	1103	8	0.4	4	0	1
	774	8				
$Se_2I_3^+$ (**A**)	1486	32	6	13	13	7
	1219	29				
$Se_6I_4^{2+}$ (**B**)	1181	104	10	65	43	22
	1096	199 [c]				
	1094					
$Se_6I_3^+$ (**C**)	1597	46	9	59	30	10
	1351	47				
	1350	47				
	1170	43				
	1007	48				
	873	42				
Se_7I^+ (**D**)	1149	101	9	68	10	10
	1064	100				
	1044	obsc.				
	998	98				
$(Se_7I)_2I^{3+}$ (**E**)	1791	44	4	61	13	13
	1637	43				
	1419	43				
	1374	44				
	1308	obsc.				
	1200	43				
	956	39				
Total			100	624	213	188

[a] The relative integrated intensities are given in arbitrary units. [b] The molar amounts of selenium, iodine, and charge have been corrected for the known enrichment of ^{77}Se-isotope (92 %) in the sample.[107] [c] Combined intensity of two overlapping resonances.

Table 6. Predicted thermodynamic outcome for main dissociation reactions of $(Se_6I_2)[AsF_6]_2$ and for loss of SO_2. Reactions numbered below with an ordinal number refer to reactions listed in the main text, those with a number prefixed by "S" refer to reactions listed in the Supporting Information.

Reaction number	**gas phase and solvated gaseous ion reaction**	$\Delta_r E^o$ **/kJ mol^{-1}**	$\Delta_r H^o$ **/kJ mol^{-1}**	$\Delta_r G^o$ **/kJ mol^{-1}**
S1	$2Se_6I_2^{2+}(g) \rightarrow Se_8^{2+}(g) + Se_4I_4^{2+}(g)$	–21.8	–21.3	–
1	$2(Se_6I_2)^{2+}(solv) \rightarrow Se_4I_4^{2+}(solv) + Se_8^{2+}(solv)$	–	–	+3.8
S2	$3Se_6I_2^{2+}(g) \rightarrow 2\ SeI_3^{2+}(g) + 2Se_8^{2+}(g)$	–216.9	–220.8	–
S3	$3Se_6I_2^{2+}(solv) \rightarrow 2\ SeI_3^{2+}(solv) + 2Se_8^{2+}(solv)$	–	–	–63.1
	solid state reactions for unsolvated salts	$\Delta_r H^o$ **/kJ mol^{-1}**	$\Delta_r S^o$ **/J K^{-1} mol^{-1}**	$\Delta_r G$**(203K)*/** $\Delta_r G^o$**(298K) /kJ mol^{-1}**
S6	$2(Se_6I_2)[AsF_6]_2(s) \rightarrow (Se_4I_4)[AsF_6]_2(s) + (Se_8)[AsF_6]_2(s)$.	-13 –13	+11 (eq (2b)) 0 (Latimer)	–15/–17 –13/–13
S22	$3(Se_6I_2)[AsF_6]_2(s) \rightarrow 2(SeI_3)[AsF_6]_2(s) + 2(Se_8)[AsF_6]_2(s)$.	+189 +189	+14 (eq (2b)) –1 (Latimer)	+186/+185 +189/+189
	solid state reactions [SO_2 in liquid (S13,S18) and gaseous (S42, S47) phases] for solvated salts	$\Delta_r H^o$ **/kJ mol^{-1}**	$\Delta_r S^o$ **/J K^{-1} mol^{-1}**	$\Delta_r G$**(203K)*/** $\Delta_r G^o$**(298K) /kJ mol^{-1}**
S13	$2(Se_6I_2)[AsF_6]_2.2SO_2(s) \rightarrow$ $(Se_4I_4)[AsF_6]_2(s) + (Se_8)[AsF_6]_2{\cdot}\frac{1}{3}SO_2$ (s). + 11/3 SO_2(l)	+60 +60 +60	+222 (eq (2b)) +210 (Latimer) +220 (eq (S6b))	+15/-6 +17/-3 +15/-6
S42	$2(Se_6I_2)[AsF_6]_2.2SO_2(s) \rightarrow$ $(Se_4I_4)[AsF_6]_2(s) + (Se_8)[AsF_6]_2{\cdot}\frac{1}{3}SO_2$ (s). + 11/3 SO_2(g)	+144 +144 +144	+542 (eq (2b)) +530 (Latimer) +539 (eq (S28b))	+34/–18 +34/–14 +34/–17
S18	$3(Se_6I_2)[AsF_6]_2.2SO_2(s) \rightarrow$ $2(Se_4I_4)[AsF_6]_2(s) + 2(Se_8)[AsF_6]_2{\cdot}\frac{1}{3}SO_2$ (s). + 16/3 SO_2(l)	+296 +296	+322 (eq (2b)) +304 (Latimer)	+230/+200 +234/+205
S47	$3(Se_6I_2)[AsF_6]_2.2SO_2(s) \rightarrow$ $2(Se_4I_4)[AsF_6]_2(s) + 2(Se_8)[AsF_6]_2{\cdot}\frac{1}{3}SO_2$ (s). + 16/3 SO_2(g)	+418 +418	+786 (eq (2b)) +769 (Latimer)	+258/+184 +262/+189
	loss of SO_2 [as liquid or gas] from solvated salts	$\Delta_r H^o$ **/kJ mol^{-1}**	$\Delta_r S^o$ **/J K^{-1} mol^{-1}**	$\Delta_r G$**(203K)*/** $\Delta_r G^o$**(298K) /kJ mol^{-1}**
3	$(Se_6I_2)[AsF_6]_2.2SO_2(s) \rightarrow (Se_6I_2)[AsF_6]_2(s) + 2SO_2(l)$	+40	+114	+17/+6
4	$(Se_6I_2)[AsF_6]_2.2SO_2(s) \rightarrow (Se_6I_2)[AsF_6]_2(s) + 2SO_2(g)$	+86	+288	+28/0
5	$Se_8[AsF_6]_2.\ \frac{1}{3}SO_2(s) \rightarrow Se_8[AsF_6]_2(s) + \frac{1}{3}SO_2(l)$	+7	+19	+3/+1
6	$Se_8[AsF_6]_2.\ \frac{1}{3}SO_2(s) \rightarrow Se_8[AsF_6]_2(s) + \frac{1}{3}SO_2(g)$	+14	+48	+4/0

* calculated using assuming that ΔrH^odoes not vary with temperature. †error in all quoted $\Delta_r G$ values are approximately ± 15 kJ mol^{-1}. In this paper $\Delta_r G$ values are compared for reactions and it is their difference (for example with respect to temperature variation) that is important rather than their absolute magnitudes. This is the basis of our discussion. For example reaction (S6) exhibits very little change in $\Delta_r G$ (S6) with respect to temperature whereas reaction (S13) is seen to have a $\Delta_r G$ (S13) value which does respond markedly to change in temperature.

Table 7. The ^{77}Se NMR spectroscopic information of 1,1,4,4-$Se_4Br_4^{2+}$ and Se_7Br^+ cations tentatively identified in the Se_4^{2+}/Br_2 system.

Species	Experimental chemical shifts (δ, ppm)			ZORA rPBE / QZ4P chemical shifts (ppm)	
	δ	Selenium atom no [a]	No of equiv. nuclei	Vacuum δ	Explicit solvent δ [b]
$Se_4Br_4^{2+}$	1596	Se2	2	1615	1596
	1126	Se1	2	1395	1126
Se_7Br^+	1317	Se4, Se5	2		
	1205	Se2, Se7	2		
	1165	Se1	1		
	1082	Se3, Se6	2		

[a] The numbering of atoms in the Se-Br cations follows that in the corresponding Se-I cations; see Figure 11 (1,1,4,4-$Se_4I_4^{2+}$), and Figure 19 (Se_7I^+). [b] Number of explicit solvent molecules in 1,1,4,4-$Se_4Br_4^{2+}$ is 2

Table 8. Summary of the known or proposed $X_mSe_n^{x+}$ cations (X = univalent group).

x	*n*	Illustrative examples	Ref.
1	1	SeX_3^+ (X = Cl, Br, I)	12, 13, 16,19
		cyclo-$Se(CR)_2^+$	116
	2	$ISeSe^+I_2$	This work
		cyclo-$(R\text{-}Se)_4^{2+}$	117
	3	$XSe_2Se^+X_2$ (X = Cl, Br)	14, 17
		$MeSeSe^+(Me)SeMe$	118
	6	(*cyclo*-$Se_6I^+)_n$	22b, 23
		$XSe_5Se^+X_2$	This work
	7	*cyclo*-Se_7X^+ (X = Br, I)	This work
	9	*cyclo*-$Se_6^+(Se_2Cl)$	15
2	2	$Se_2I_4^{2+}$	20
	4	$Se_4I_4^{2+}$	21
	6	*cyclo*-$Se_6I_2^{2+}$	22
		cyclo-$Se_6Ph_2^{2+}$	119
		$I_2Se^+Se_4Se^+I_2$	This work
3	14	*cyclo*-$\{(Se_7I)_2I\}^+$	This work

Figure Captions

Figure 1. The 1,4-$Se_6I_2^{2+}$ cation in $(Se_6I_2)[AsF_6]_2 \cdot 2SO_2$.[22]

Figure 2. Valence bond structures describing the charge delocalization and bond alternation in 1,4-$Se_6I_2^{2+}$.[22]

Figure 3. The ^{77}Se NMR spectrum of the equilibrium SO_2(l) solution of $(Se_6I_2)[AsF_6]_2 \cdot 2SO_2$ at -70 °C involving selenium enriched in the ^{77}Se isotope (enrichment 92 %). Inserts represent portions of the ^{77}Se NMR spectrum of the natural abundance sample.

Figure 4. PS-DQF ^{77}Se-^{77}Se COSY spectrum of the equilibrium solution of $(Se_6I_2)[AsF_6]_2 \cdot 2SO_2$ at -70 °C involving selenium enriched in the ^{77}Se isotope (enrichment 92 %).

Figure 5. The optimized structure of SeI_3^+ (**2**). Bond lengths are given in Ångströms. Relative AIM bond orders (bold italic) [86] and natural charges (bold) are also given.

Figure 6. The effect of explicit solvent molecules on the ^{77}Se NMR chemical shift of SeI_3^+. **(a)** no solvent model (COSMO solvent model only 1371 ppm), **(b)** one SO_2 coordinated to selenium, **(c)** one SO_2 coordinated to iodine, **(d)** three SO_2 coordinated to iodine, **(e)** three SO_2 coordinated to iodine and one SO_2 coordinated to selenium.

Figure 7. The observed and simulated ^{77}Se NMR spectra of different isotopomers of 1,4-$Se_6I_2^{2+}$.

Figure 8. The optimized structures of the *endo,endo* (**1₁**) and *exo,exo* (**1₂**) conformations of 1,4-$Se_6I_2^{2+}$. Bond lengths are given in Ångströms. For the **1₁** conformation AIM critical points (black dots), relative AIM bond orders (bold italic) [86] and natural charges (bold) are also given.

Figure 9. $p^2 \rightarrow \sigma^*$ electron transfer in 1,4-$Se_6I_2^{2+}$ leading to bond alternation within the selenium ring and the partial Se-I π bonds.

Figure 10. The observed and simulated ^{77}Se NMR spectra of different isotopomers of 1,1,4,4-$Se_4I_4^{2+}$.

Figure 11. The optimized structure of 1,1,4,4-$Se_4I_4^{2+}$ (**3**) and the $p^2 \rightarrow \sigma^*$ electron transfer in the cation (insert). AIM critical points are shown in black dots. Bond lengths (in Ångströms), relative AIM bond orders (bold italic),[86] and natural charges (bold) are also given.

Figure 12. The optimized structures of Se_8^{2+} (**5**) and Se_{10}^{2+} (**6**). Optimized bond lengths and experimental bond lengths (italic) are given in Ångströms.[97,98] Relative AIM bond orders (bold italic) [86] and natural charges (bold) are also shown.

Figure 13. Observed chemical shifts of Group **A** resonances.

Figure 14. Observed and simulated chemical shifts of Group **B** resonances.

Figure 15. Observed and simulated chemical shifts of Group **C** resonances.

Figure 16. Observed and simulated chemical shifts of Group **D** resonances.

Figure 17. Observed and simulated chemical shifts of Group **E** resonances.

Figure 18. The optimized structures of (a) 1,1,2-$Se_2I_3^+$ (**7**), (b) three conformations of 1,1,6,6-$Se_6I_4^{2+}$ (**8₁**), and (c) two conformations of 1,1,6-$Se_6I_3^+$ (**9₁**). Bond lengths (Å), relative AIM bond orders (bold italic) [86] [for 1,1,2-$Se_2I_3^+$ relative Mayer bond orders are given in parentheses],[102] natural charges (bold), relative free energies of conformations in SO_2,[91] and assignments of the ^{77}Se NMR resonances are given.

Figure 19. The optimized structures of four low energy conformations of Se_7I^+. Structural parameters (Å), relative AIM bond orders (bold italic),[86] natural charges (bold), relative free energies in SO_2,[91] and assignments of the ^{77}Se NMR resonances are shown.

Figure 20. The optimized structure of (4-Se_7I)I^{3+} (**11**). Bond lengths (Å) and assignments of the ^{77}Se NMR resonances are given.

Figure 21. Summary of the ^{77}Se chemical shift assignments.

Figure 22. The trends in $^1J_{SeSe}$ in 1,4-$Se_6I_2^{2+}$, 1,1,4,4-$Se_4I_4^{2+}$, 1,1,6-$Se_6I_3^+$, and (4-Se_7I)$_2I^{3+}$.

Scheme 1. Bond alternation arising from charge delocalization (l = long, s = short)

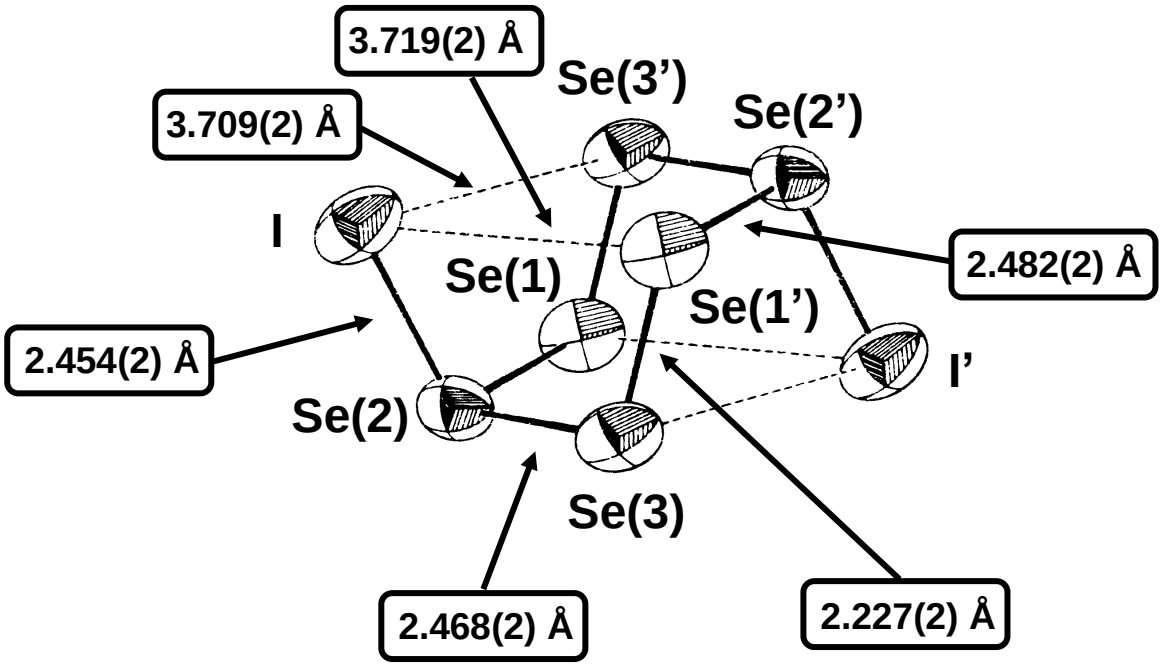
3.719(2) Å
Se(3')
3.709(2) Å
Se(2')
I
Se(1)
2.482(2) Å
Se(1')
2.454(2) Å
I'
Se(2)
Se(3)
2.468(2) Å
2.227(2) Å

Figure 1

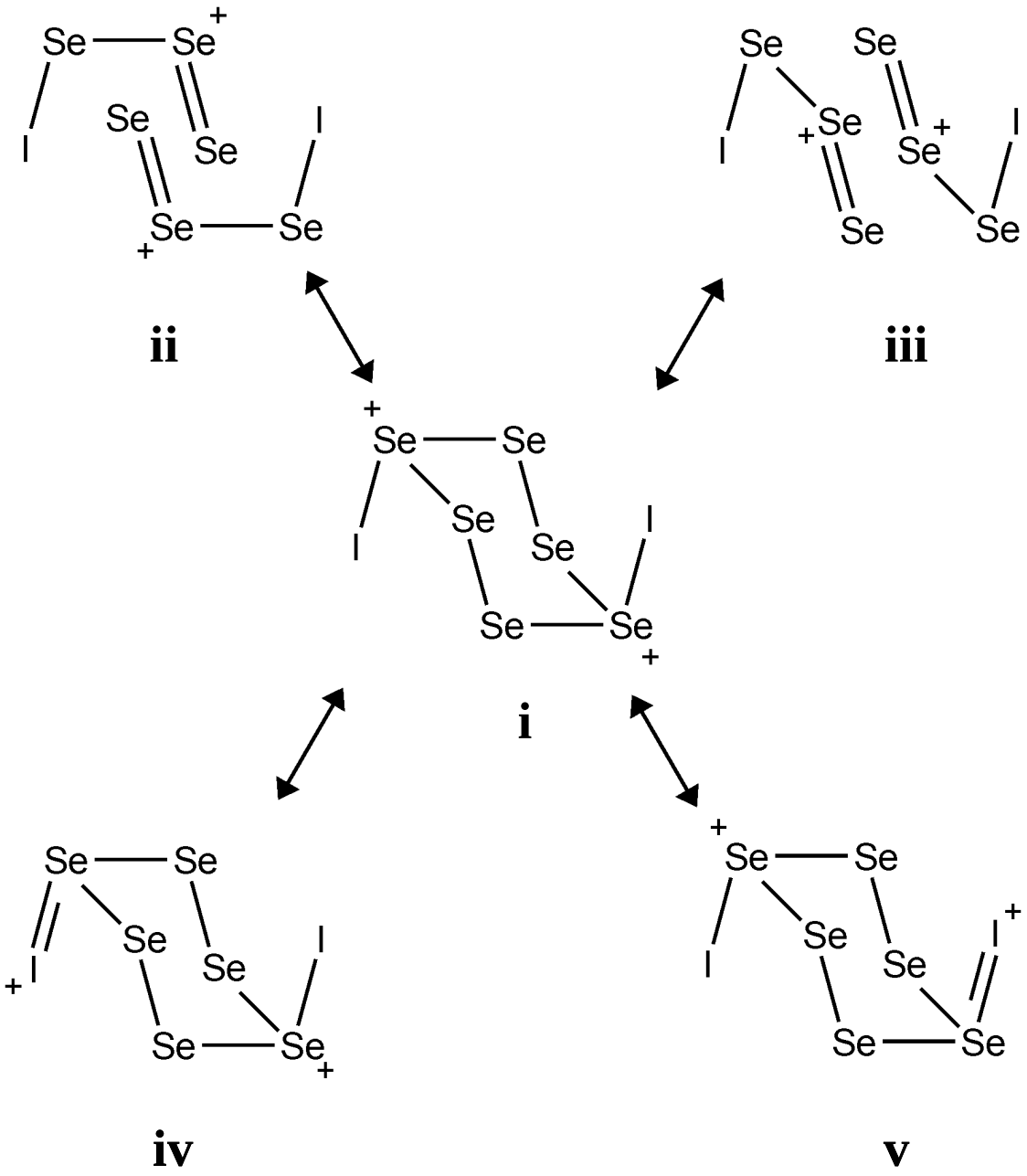

Figure 2

Figure 3

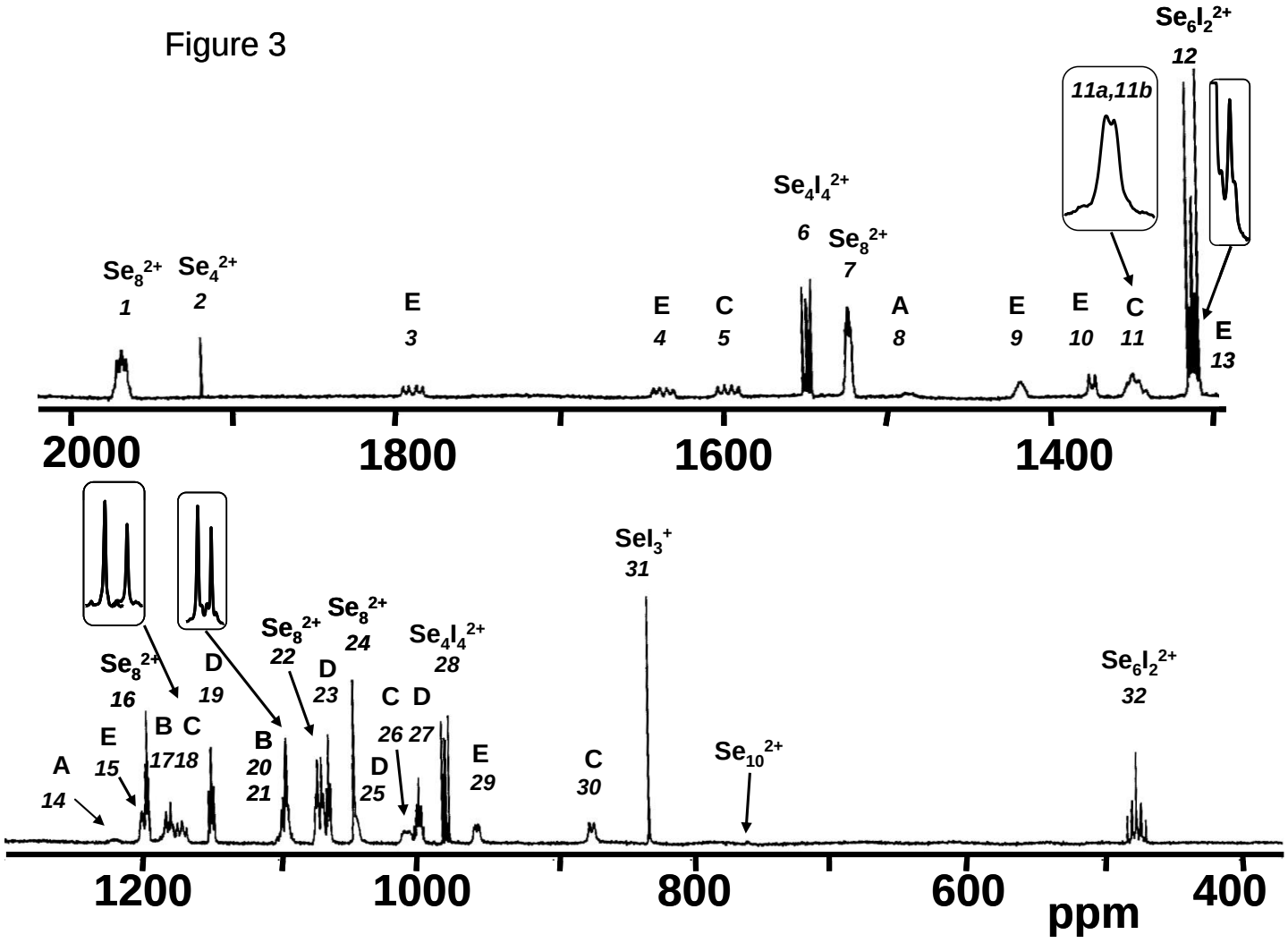
Se6I2 2+
12
11a,11b
Se4I4 2+
6
Se8 2+
7
Se8 2+
1
Se4 2+
2
E
3
E
4
C
5
A
8
E
9
E
10
C
11
E
13
2000
1800
1600
1400
SeI3 +
31
Se8 2+
16
D
19
Se8 2+
22
Se8 2+
24
D
23
Se4I4 2+
28
Se6I2 2+
32
E
15
B C
17 18
B
20
21
C D
26 27
A
14
D
25
E
29
C
30
Se10 2+
1200
1000
800
600
ppm
400

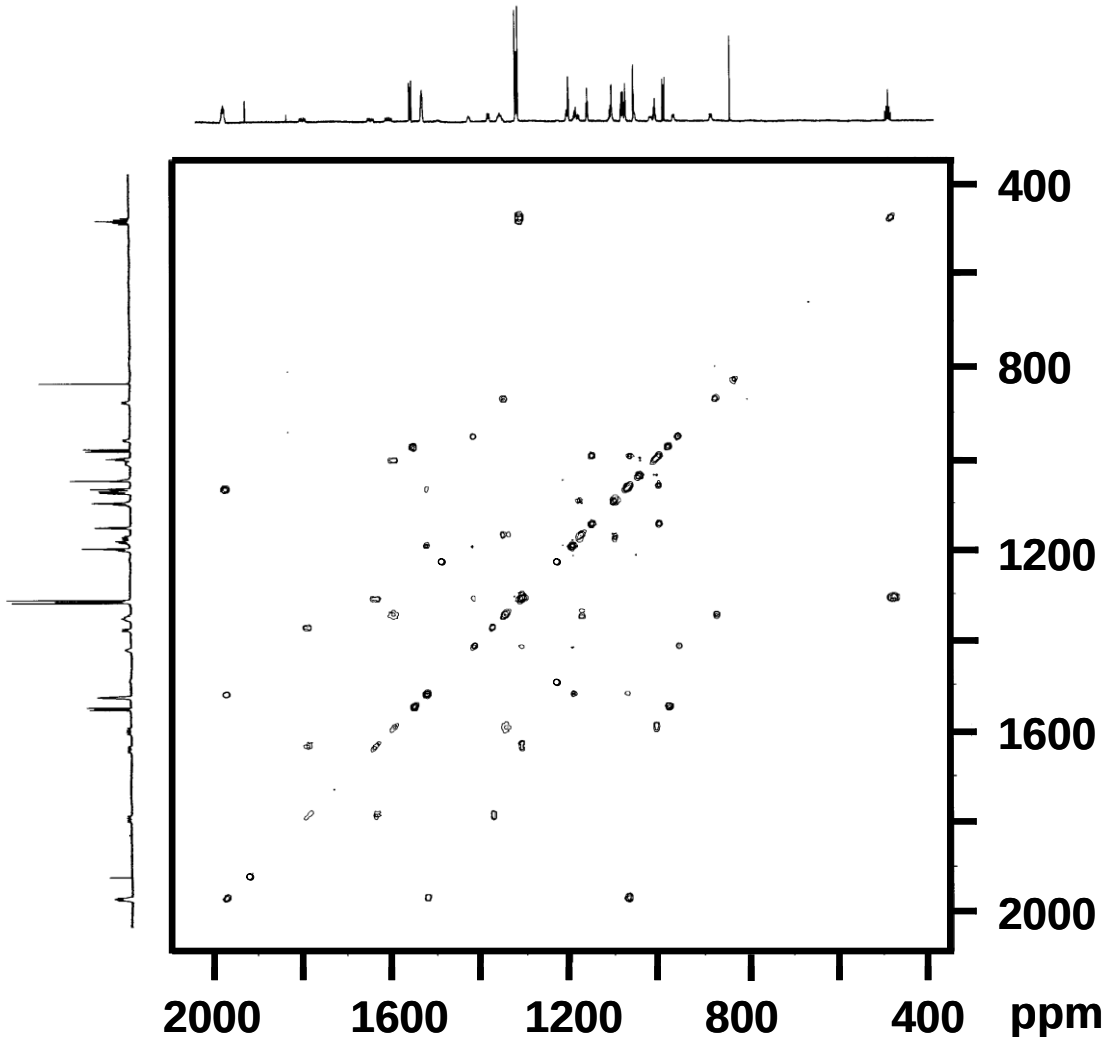

Figure 4

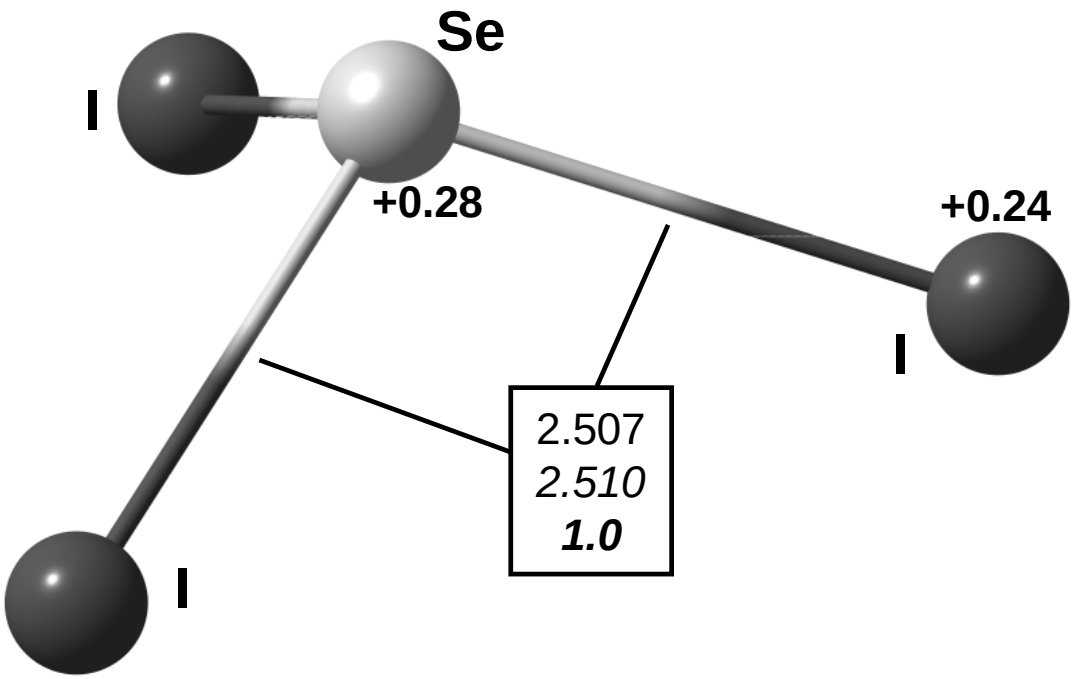

Figure 5

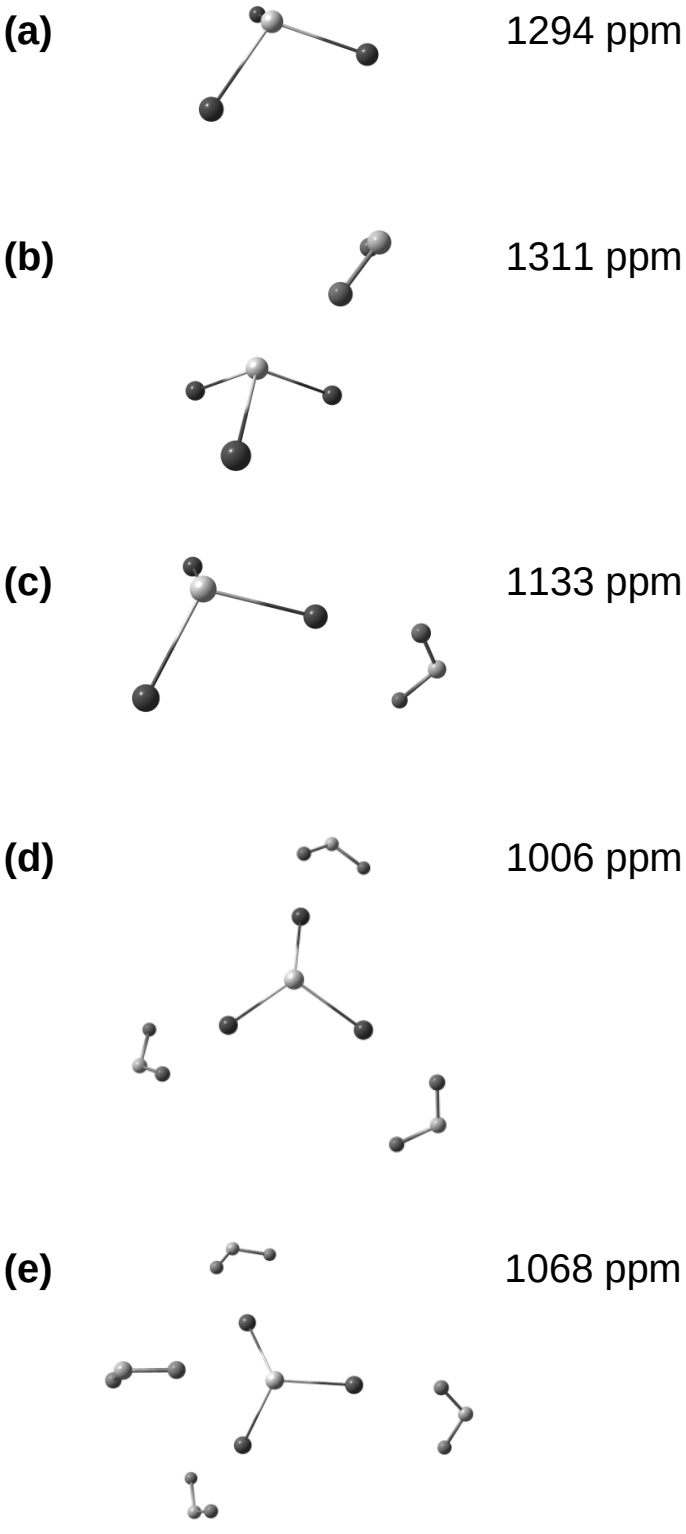

Figure 6

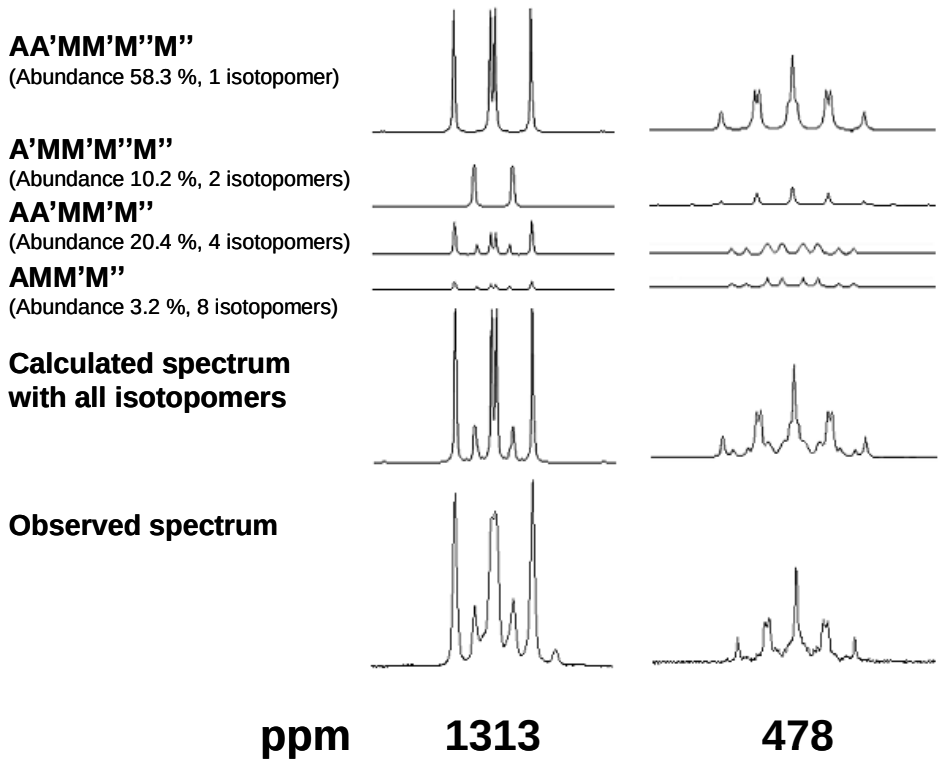
AA'MM'M''M''
(Abundance 58.3 %, 1 isotopomer)
A'MM'M''M''
(Abundance 10.2 %, 2 isotopomers)
AA'MM'M''
(Abundance 20.4 %, 4 isotopomers)
AMM'M''
(Abundance 3.2 %, 8 isotopomers)
Calculated spectrum with all isotopomers
Observed spectrum
ppm
1313
478

Figure 7

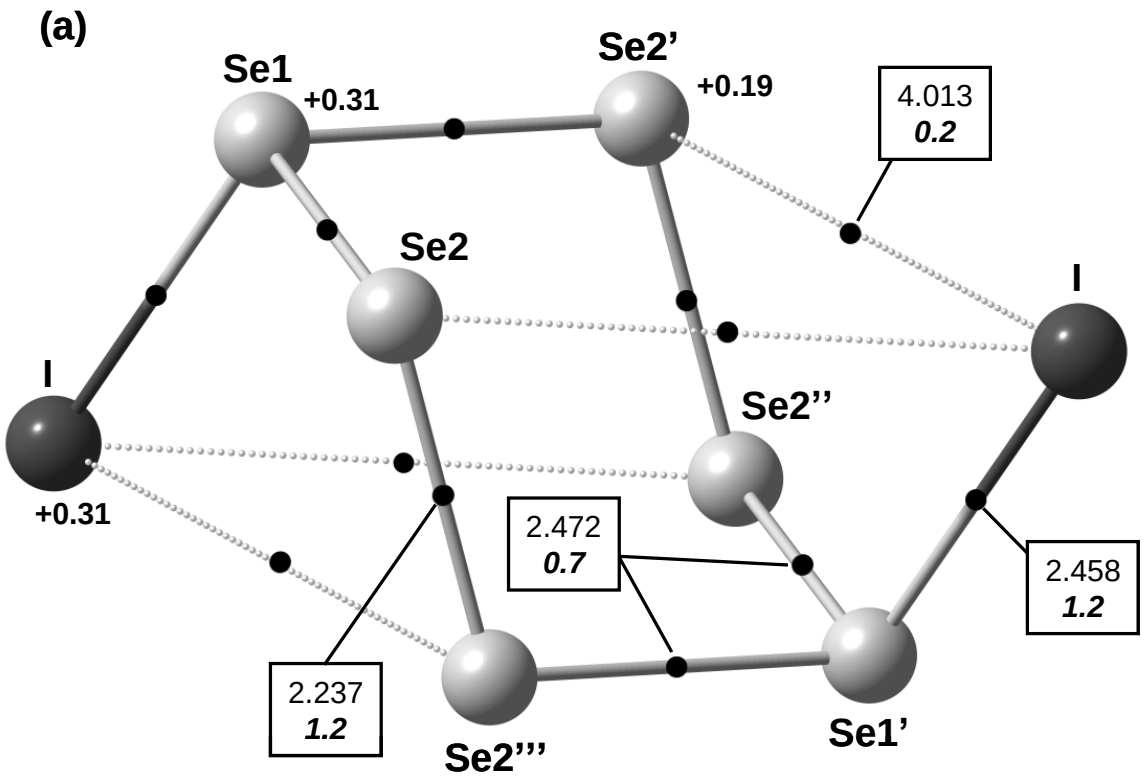

Conformation $\mathbf{1_1}$

Figure 8(a)

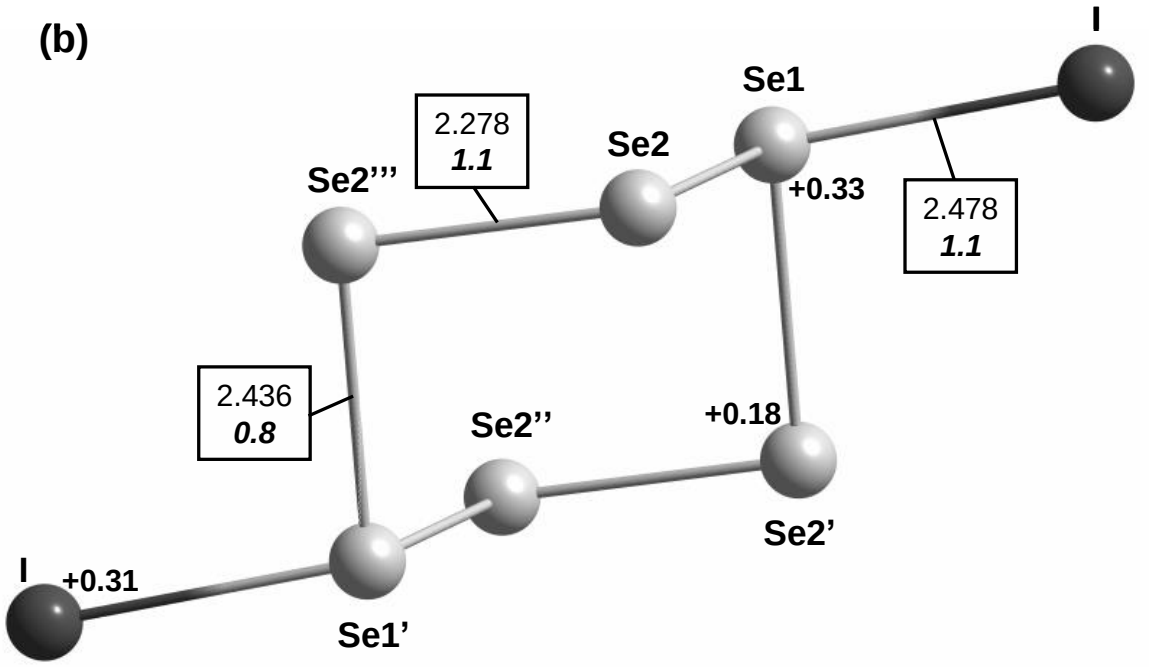

Conformation $\mathbf{1}_2$

Figure 8(b)

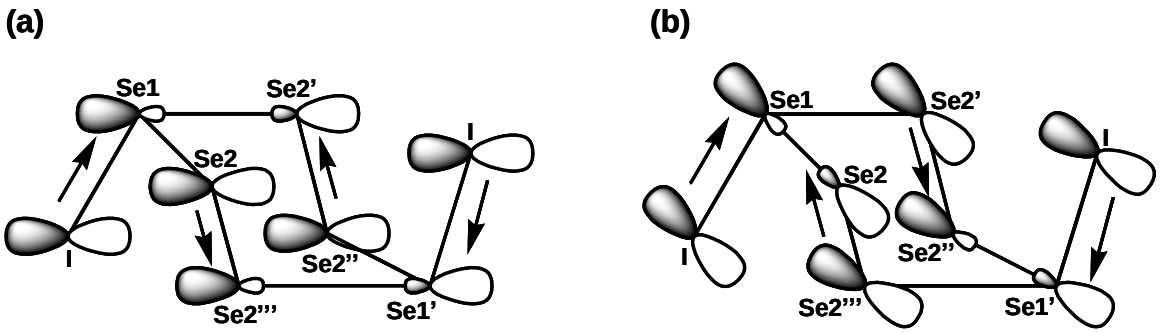

Figure 9

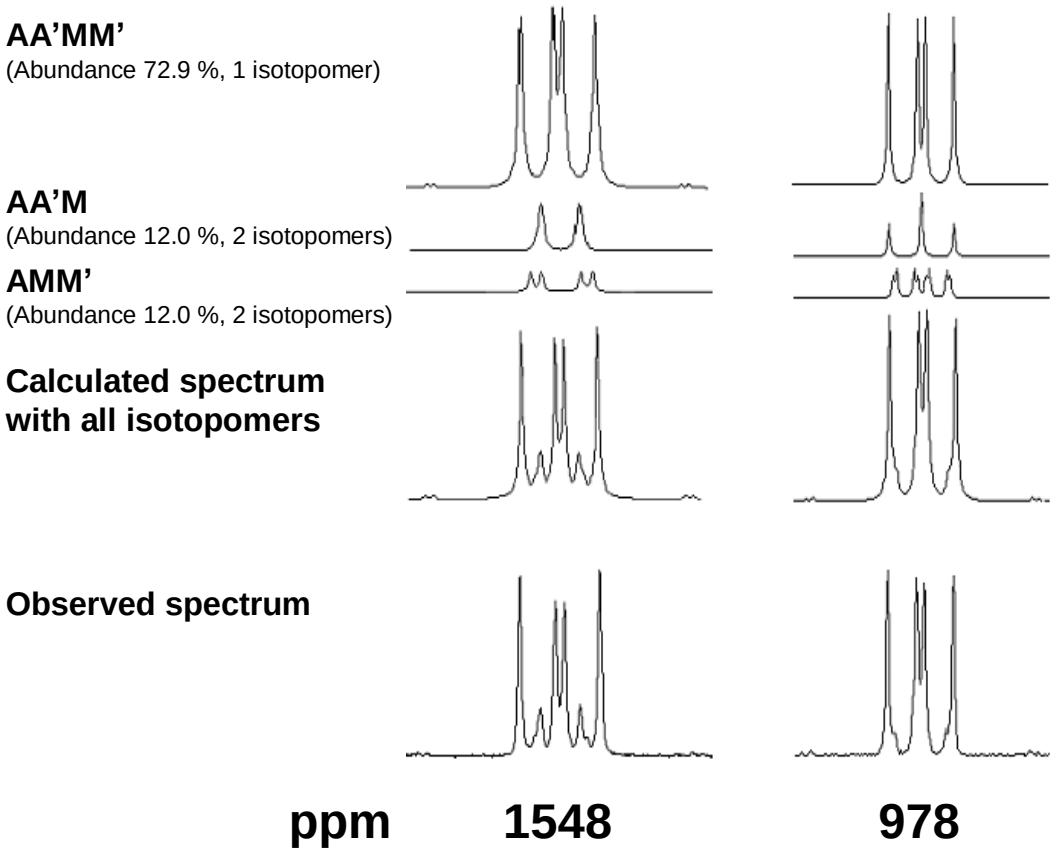
AA'MM'
(Abundance 72.9 %, 1 isotopomer)
AA'M
(Abundance 12.0 %, 2 isotopomers)
AMM'
(Abundance 12.0 %, 2 isotopomers)
Calculated spectrum
with all isotopomers
Observed spectrum
ppm
1548
978

Figure 10

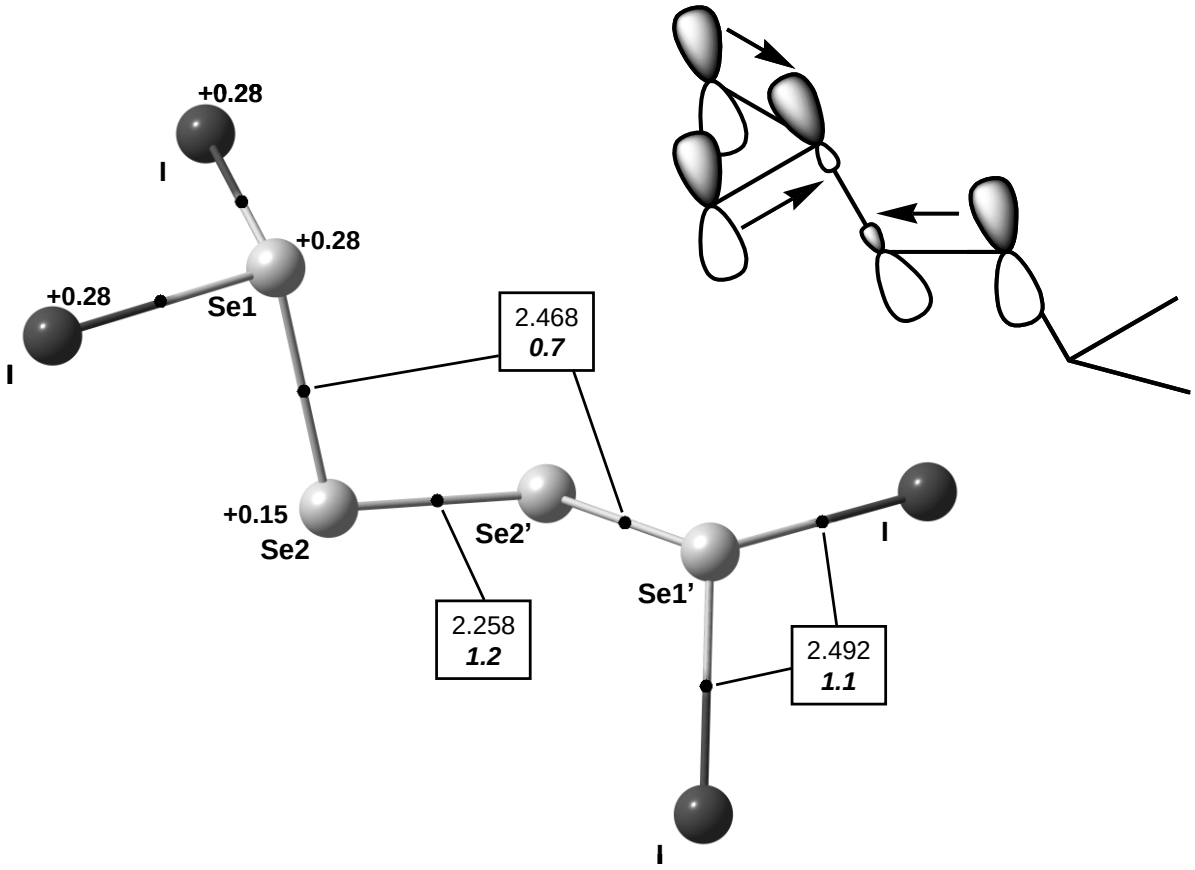

Figure 11

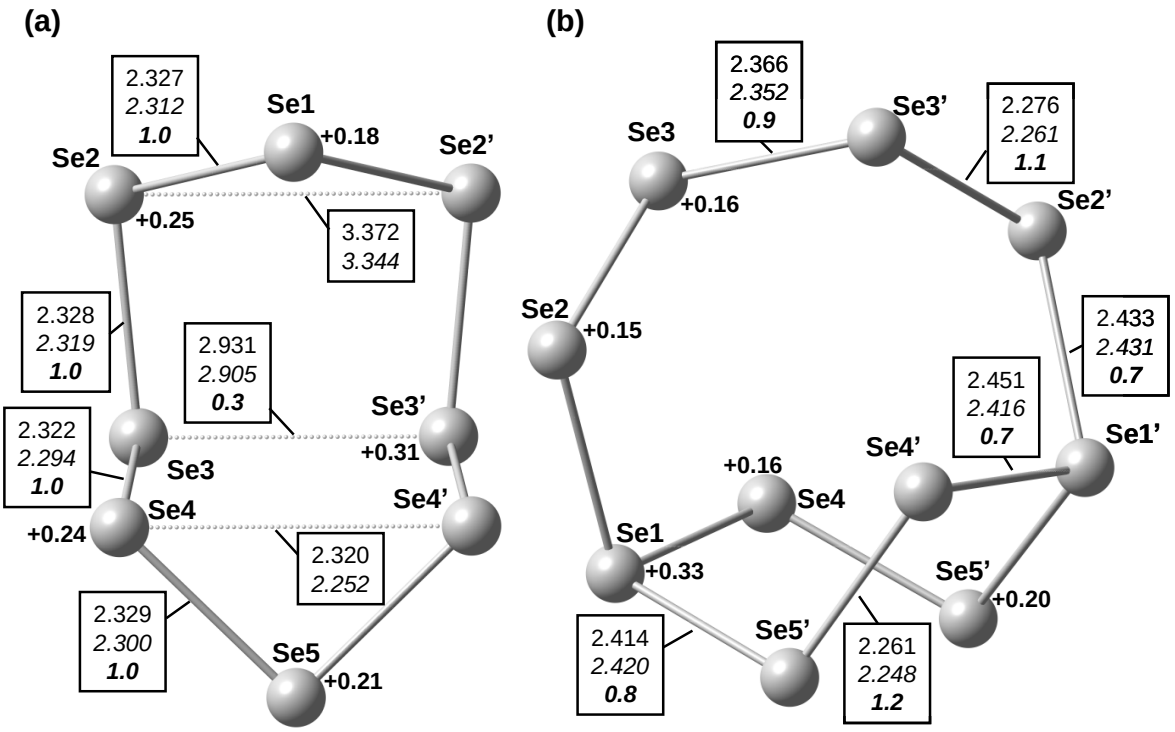
(a)
2.327
2.312
1.0
Se1
+0.18
Se2
Se2'
+0.25
3.372
3.344
2.328
2.319
1.0
2.931
2.905
0.3
Se3'
2.322
2.294
1.0
Se3
+0.31
Se4
Se4'
+0.24
2.320
2.252
2.329
2.300
1.0
Se5
+0.21
(b)
2.366
2.352
0.9
Se3
Se3'
2.276
2.261
1.1
+0.16
Se2'
Se2
+0.15
2.433
2.431
0.7
2.451
2.416
0.7
Se1'
Se4'
+0.16
Se4
Se1
+0.33
Se5'
+0.20
2.414
2.420
0.8
Se5'
2.261
2.248
1.2

Figure 12

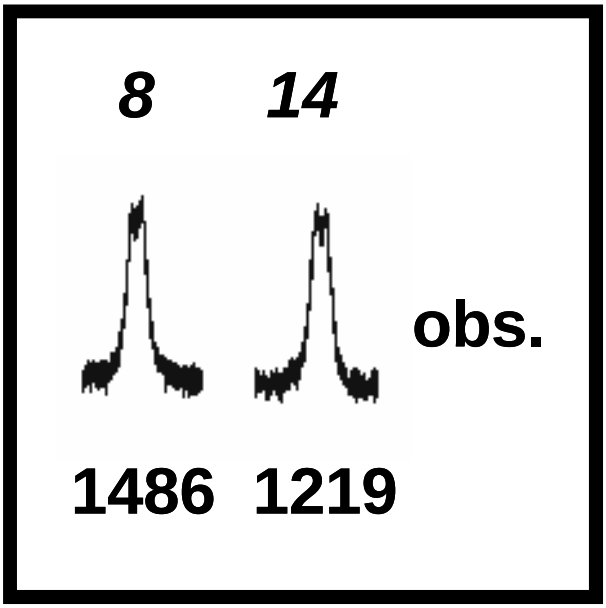

Figure 13

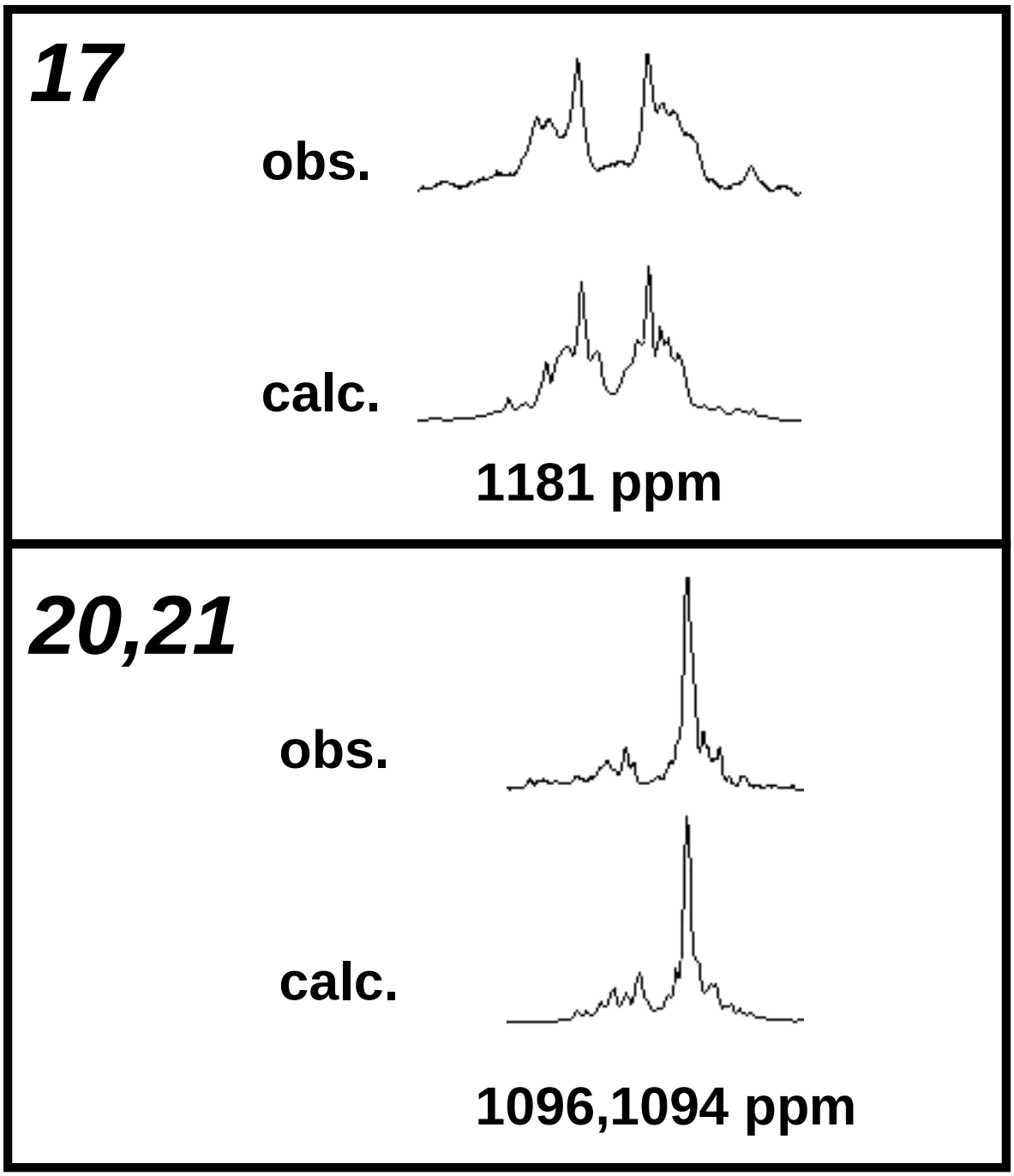

Figure 14

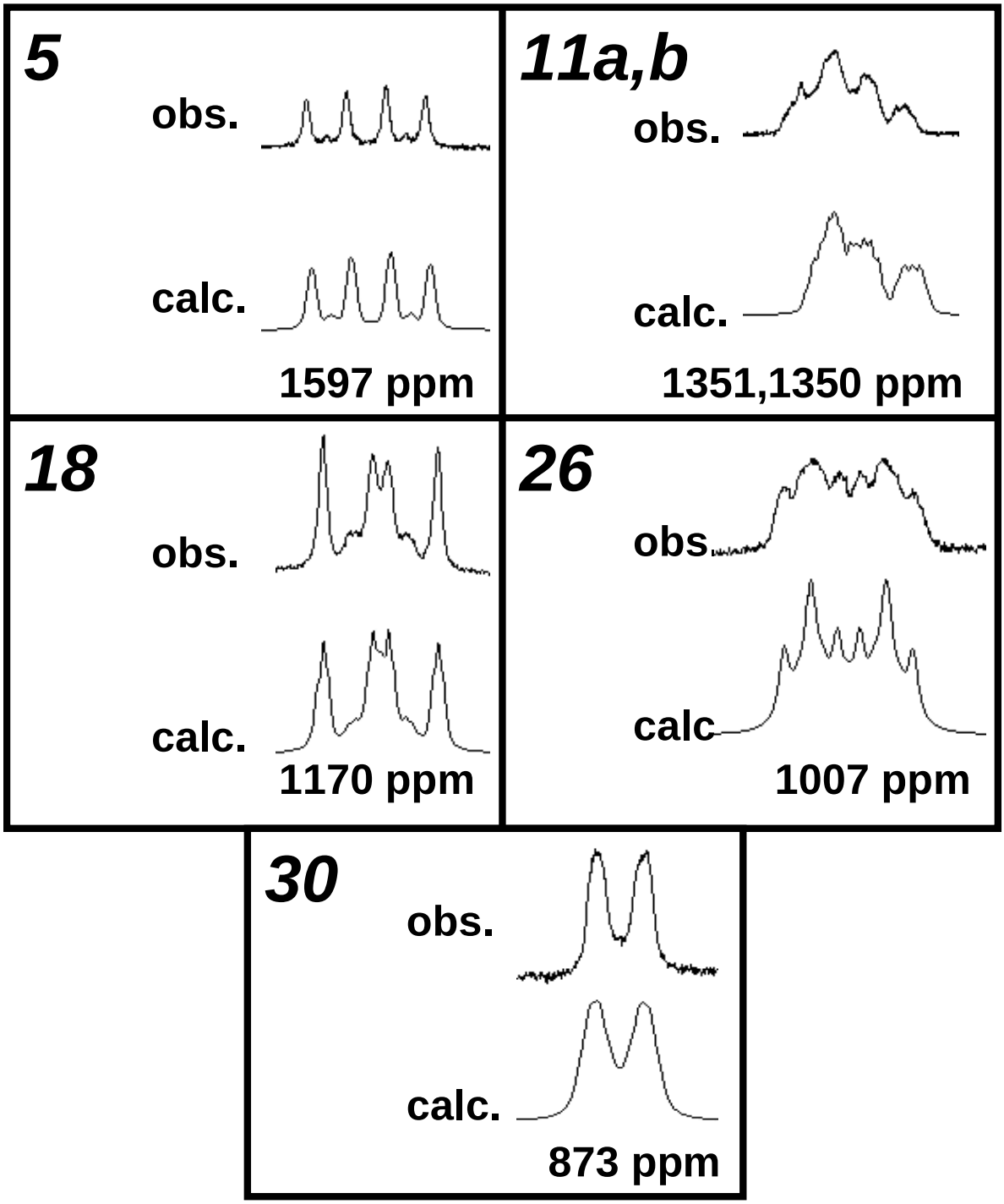
5
obs.
calc.
1597 ppm
11a,b
obs.
calc.
1351,1350 ppm
18
obs.
calc.
1170 ppm
26
obs
calc
1007 ppm
30
obs.
calc.
873 ppm

Figure 15

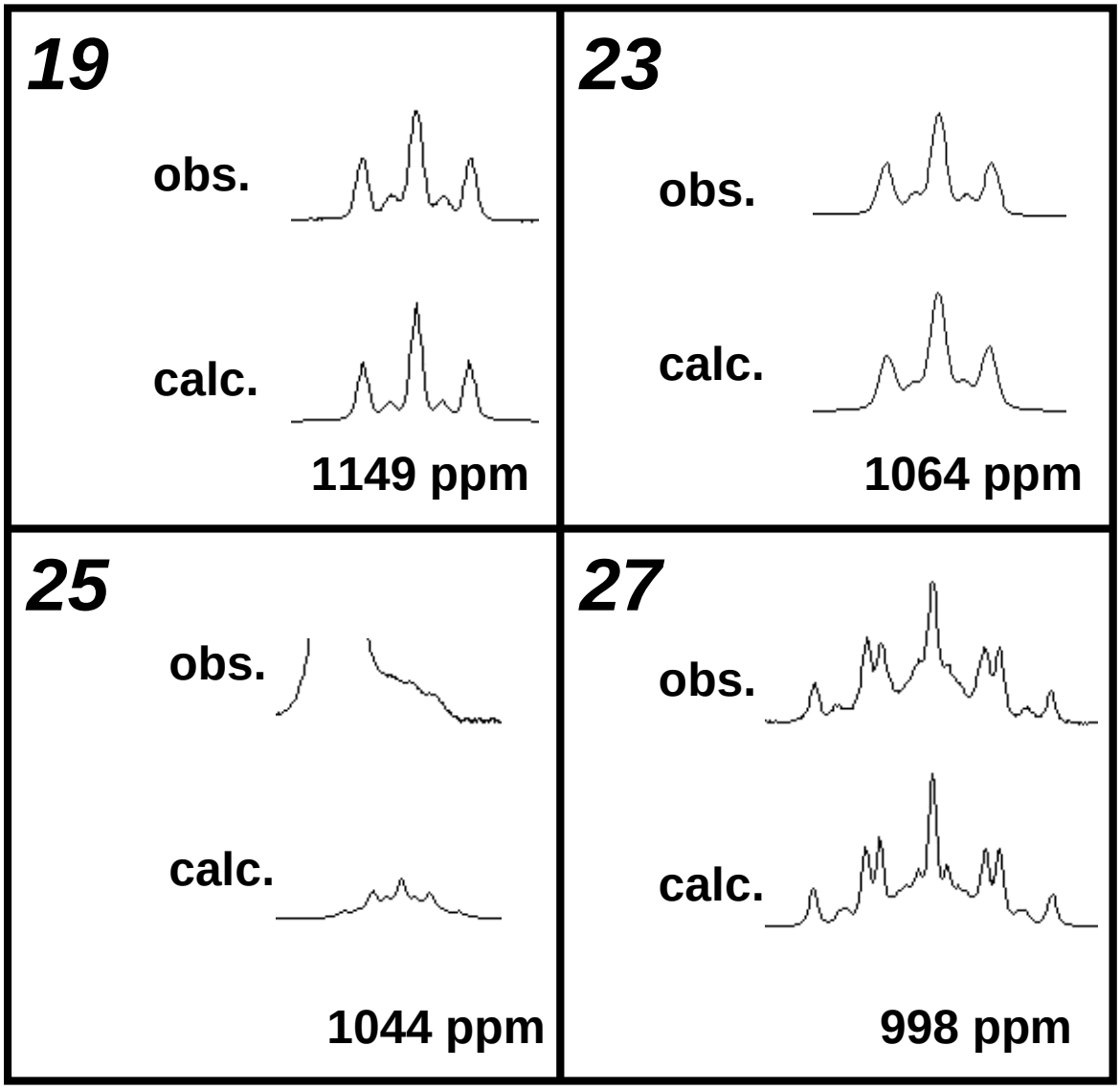
19
obs.
calc.
1149 ppm
23
obs.
calc.
1064 ppm
25
obs.
calc.
1044 ppm
27
obs.
calc.
998 ppm

Figure 16

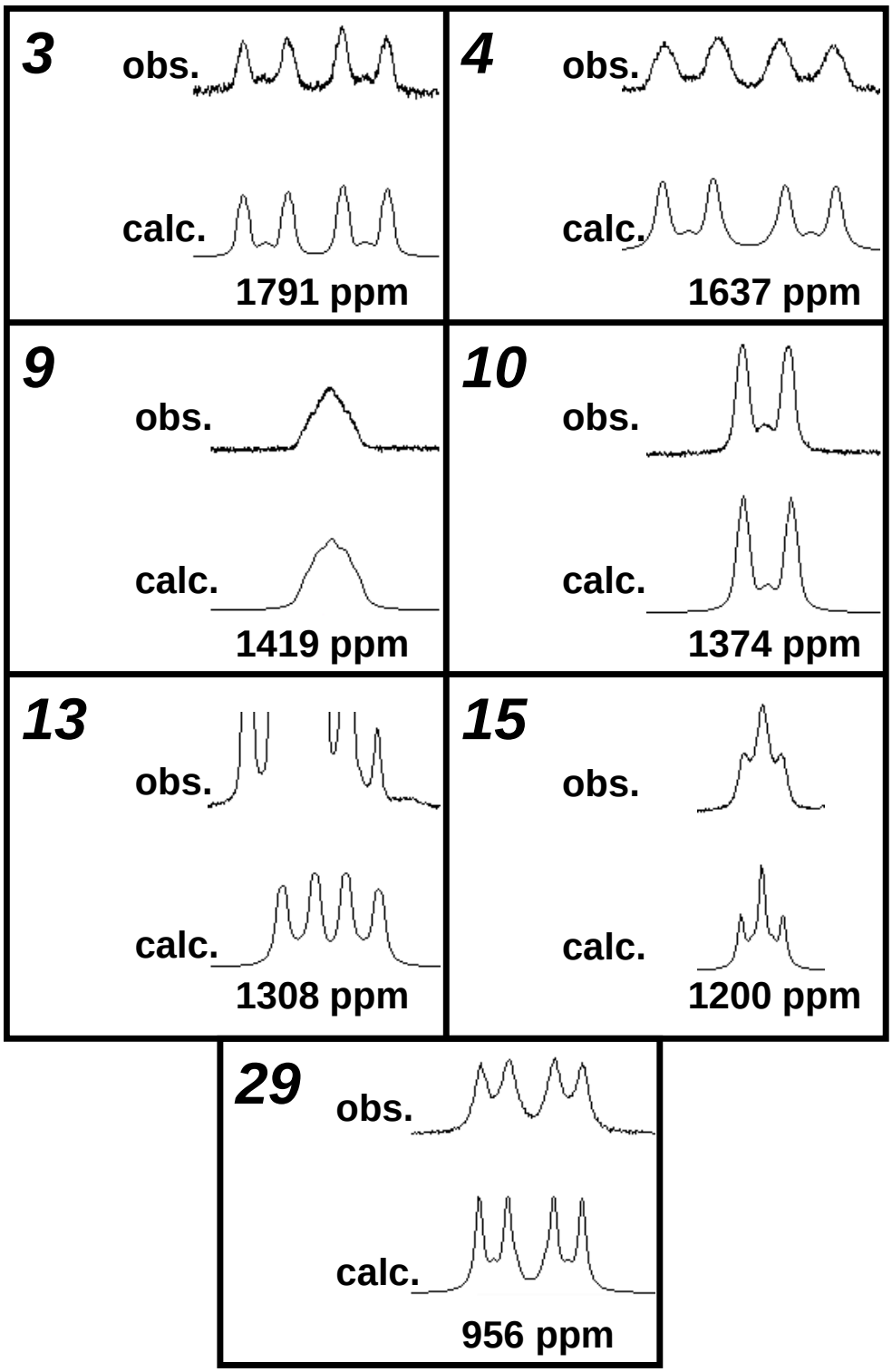
3
obs.
calc.
1791 ppm
4
obs.
calc.
1637 ppm
9
obs.
calc.
1419 ppm
10
obs.
calc.
1374 ppm
13
obs.
calc.
1308 ppm
15
obs.
calc.
1200 ppm
29
obs.
calc.
956 ppm

Figure 17

(a)

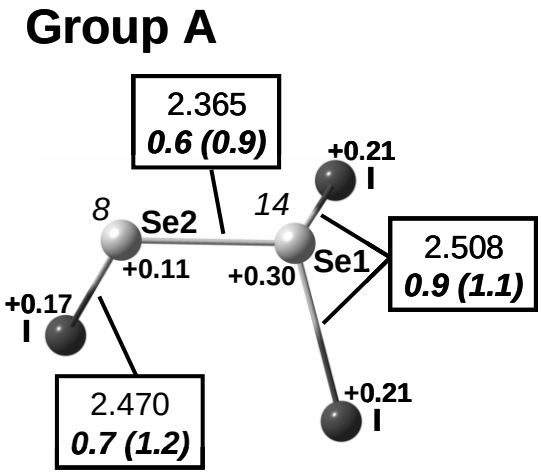

7

Figure 18(a)

(b)

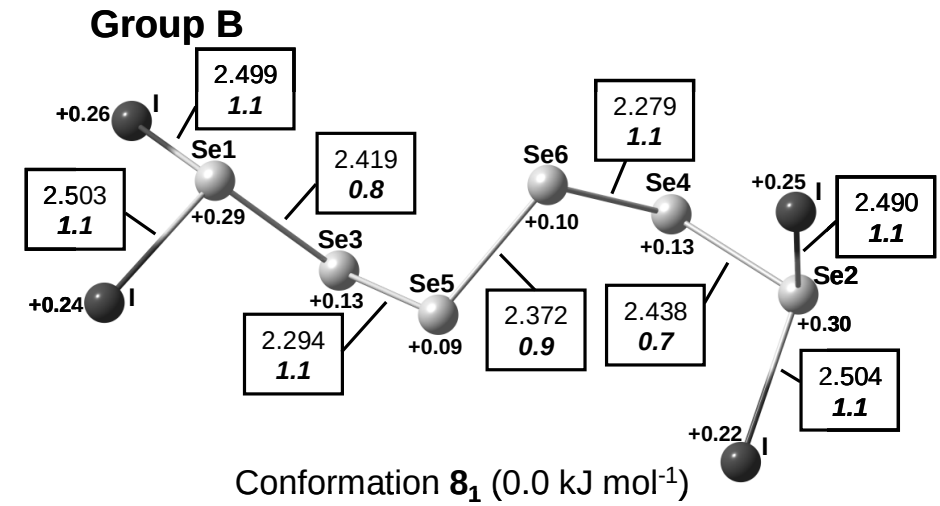

Conformation $\mathbf{8_1}$ (0.0 kJ mol^{-1})

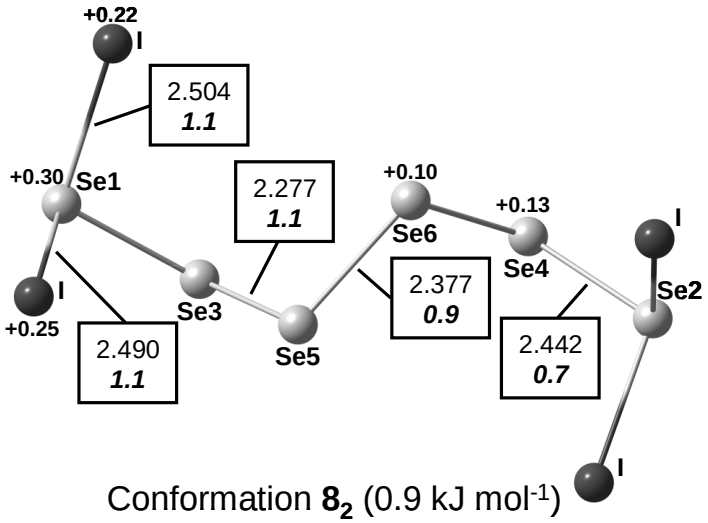

Conformation $\mathbf{8_2}$ (0.9 kJ mol^{-1})

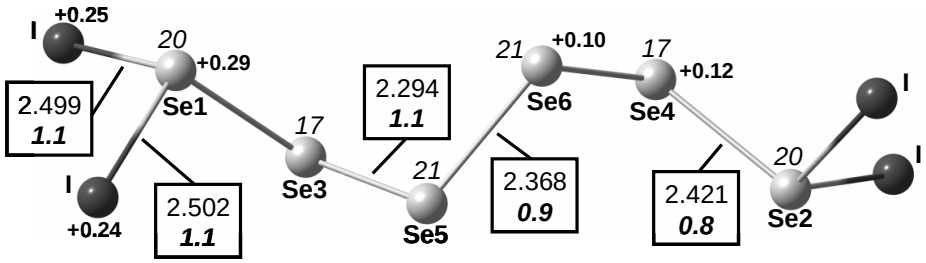

Conformation $\mathbf{8_3}$ (5.7 kJ mol^{-1})

Figure 18(b)

(c)

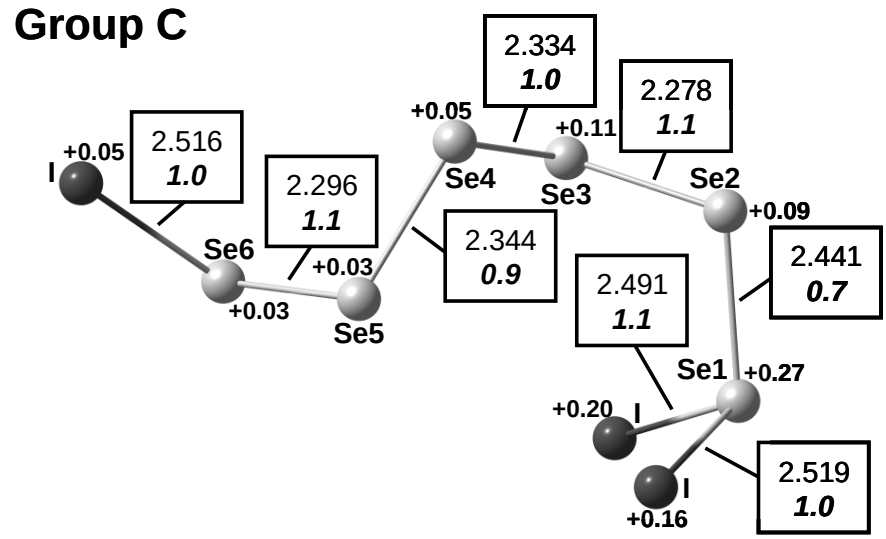

Conformation $\mathbf{9_1}$ (0.0 kJ mol^{-1})

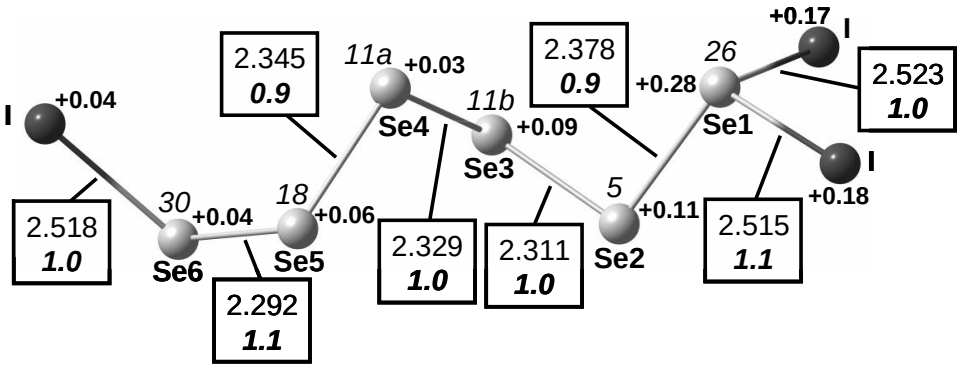

Conformation $\mathbf{9_2}$ (4.0 kJ mol^{-1})

Figure 18(c)

Group D

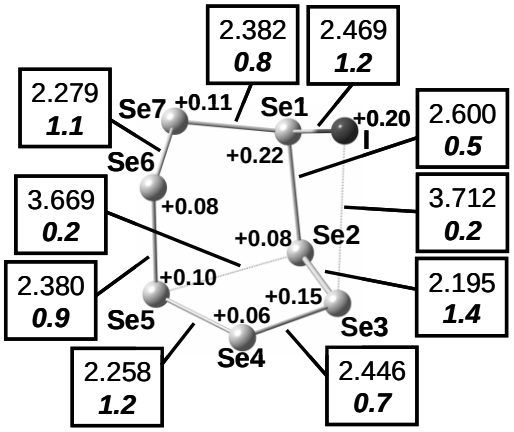

Conformation **10**$_1$ (0.0 kJ mol^{-1})

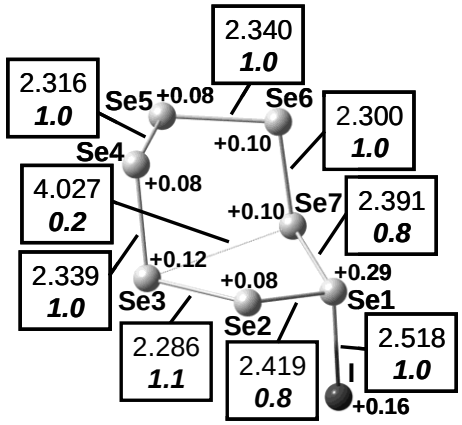

Conformation **10**$_2$ (1.9 kJ mol^{-1})

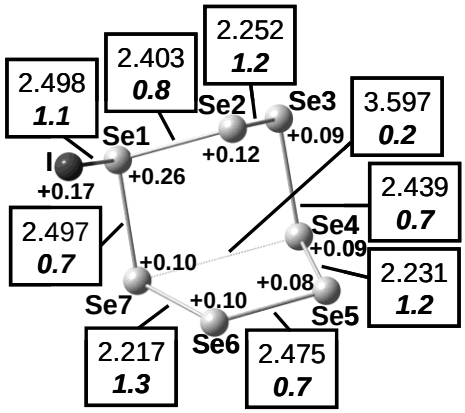

Conformation **10**$_3$ (8.9 kJ mol^{-1})

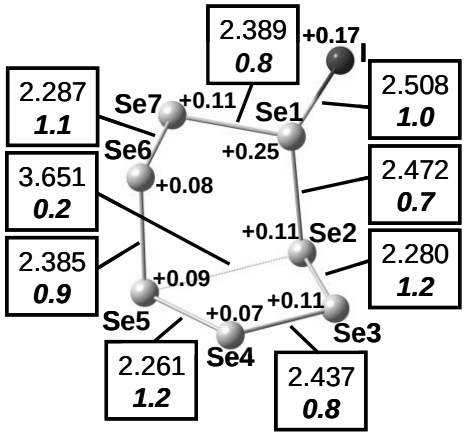

Conformation **10**$_4$ (12.2 kJ mol^{-1})

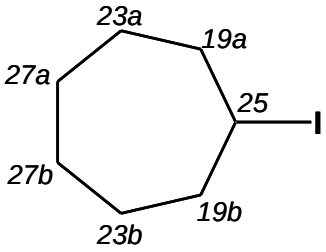

Figure 19

Group E

(11)

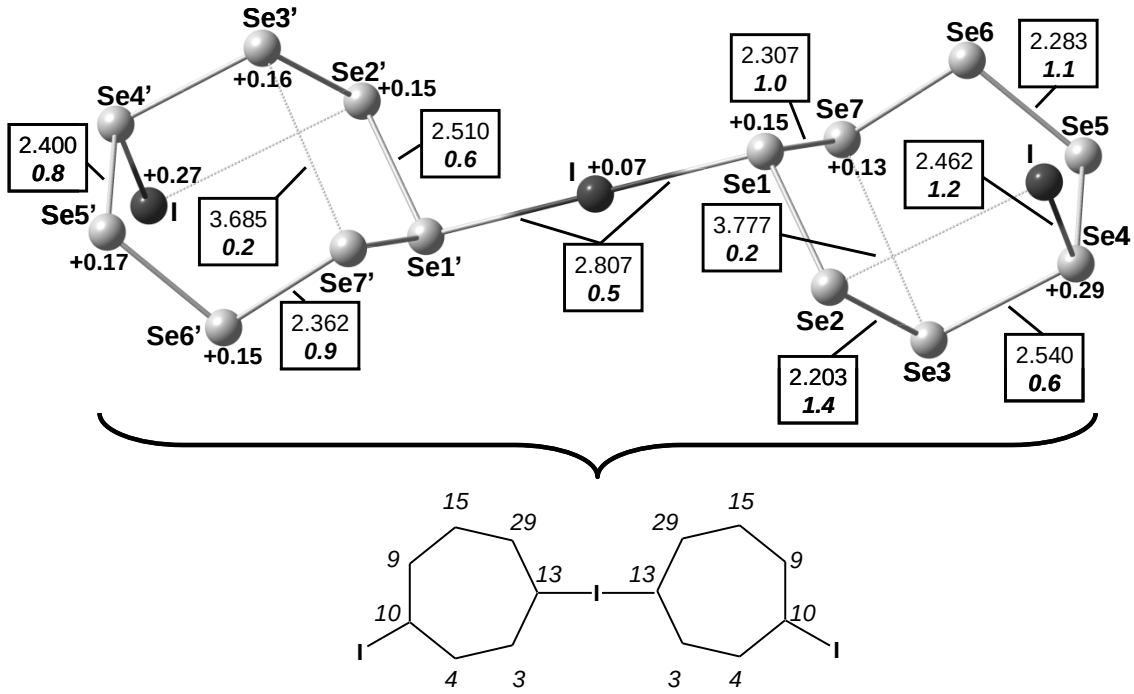

Figure 20

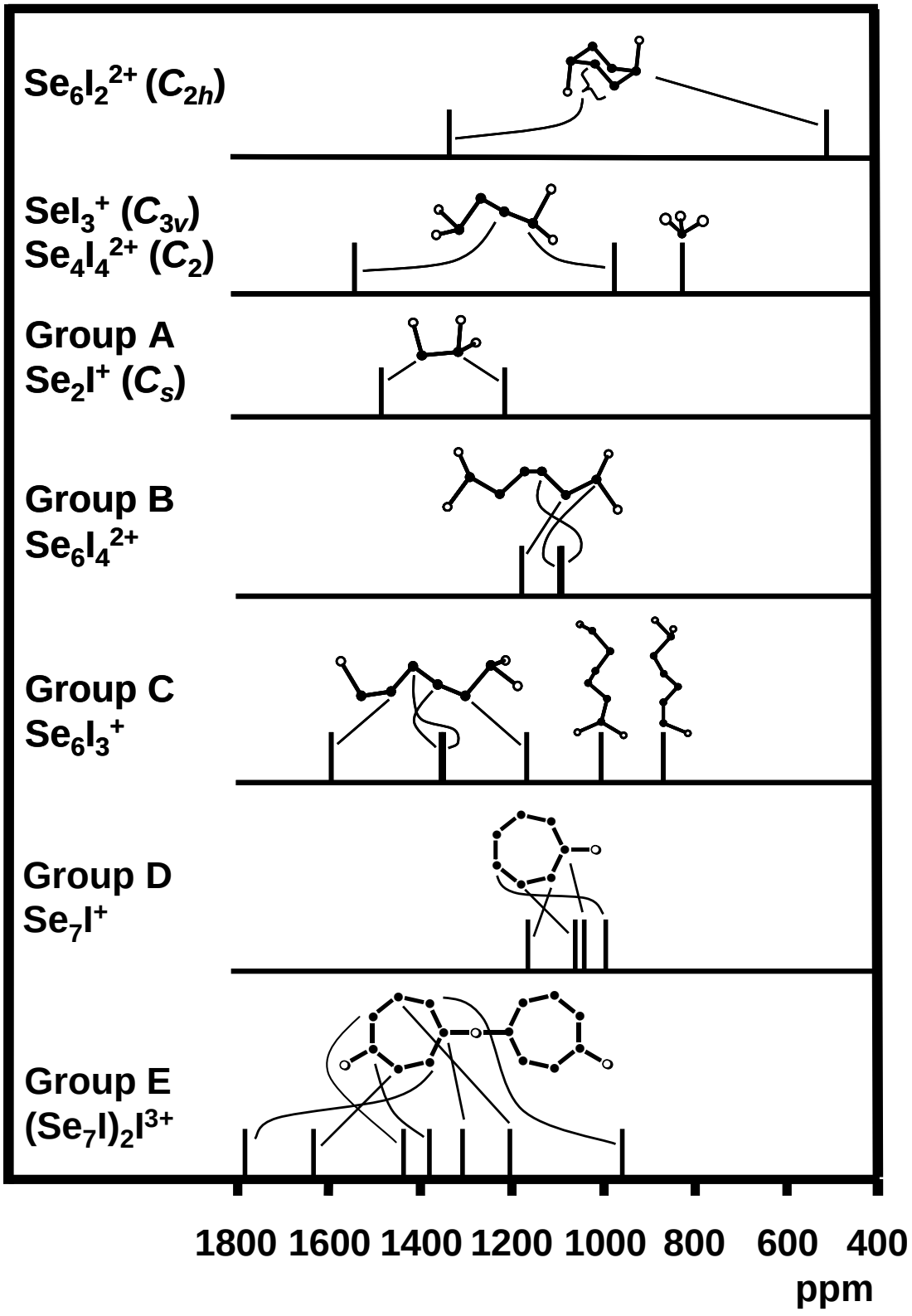
$Se_6I_2^{2+}$ (C_{2h})
SeI_3^+ (C_{3v})
$Se_4I_4^{2+}$ (C_2)
Group A
Se_2I^+ (C_s)
Group B
$Se_6I_4^{2+}$
Group C
$Se_6I_3^+$
Group D
Se_7I^+
Group E
$(Se_7I)_2I^{3+}$
1800 1600 1400 1200 1000 800 600 400
ppm

Figure 21

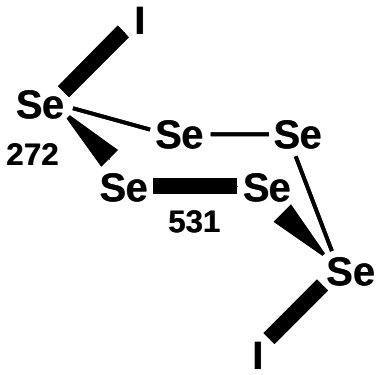

1,4-$Se_6I_2^{2+}$

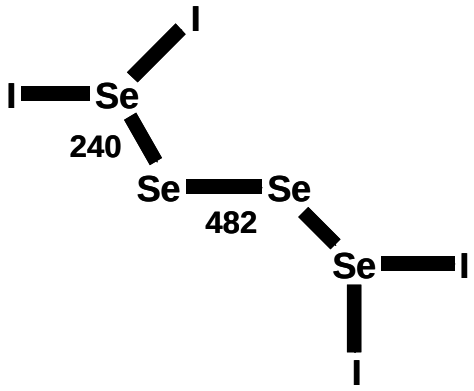

1,1,4,4-$Se_4I_4^{2+}$

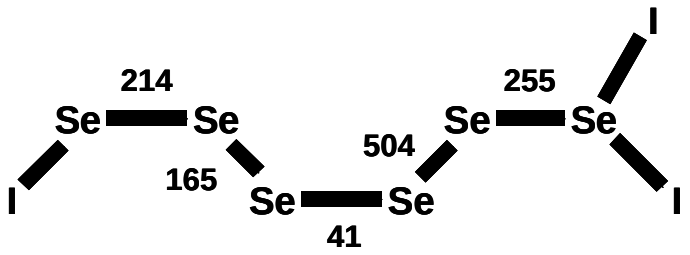

1,1,6-$Se_6I_3^{+}$

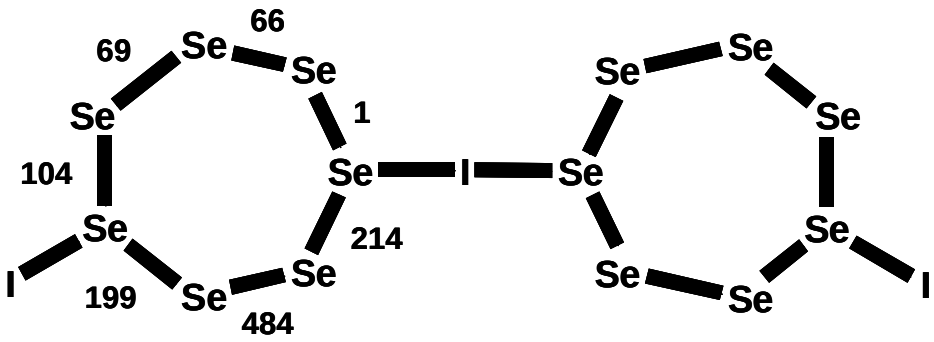

$(4\text{-}Se_7I)_2I^{3+}$

Figure 22

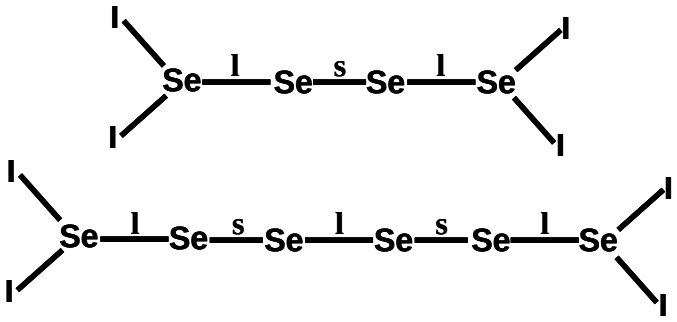

Scheme 1